Ore Geology Reviews 106 (2019) 12–27

Contents lists available at ScienceDirect

Ore Geology Reviews

journal homepage: www.elsevier.com/locate/oregeorev

Diversity of lithium mica compositions in mineralized granite–greisen system: Cínovec Li-Sn-W deposit, Erzgebirge

Karel Breiter[a,*], Michaela Hložková[b], Zuzana Korbelová[a], Michaela Vašinová Galiová[c,d]

[a] Institute of Geology of the Czech Academy of Science, Rozvojová 269, CZ-165 00 Praha 5, Czech Republic
[b] Department of Chemistry, Faculty of Science, Masaryk University, Kotlářská 2, CZ-611 37 Brno, Czech Republic
[c] Institute of Chemistry and Technology of Environmental Protection, Faculty of Chemistry, Brno University of Technology, Purkyňova 118, 61200 Brno, Czech Republic
[d] Central European Institute of Technology, Brno University of Technology, Purkyňova 123, 61200 Brno, Czech Republic

ARTICLE INFO

Keywords:
Li-mica
Trace elements
Granite
Greisen
Cínovec/Zinnwald
Krušné Hory/Erzgebirge

ABSTRACT

The Li-Sn-W deposit Cínovec/Zinnwald in the eastern Erzgebirge (Czech Republic and Germany) represents one of the worldwide best known examples of complex rare-metal plutons with pervasive greisenization. Mica from altogether 38 samples representing all granite and greisen varieties from the present surface to the depth of 1596 m was analysed using electron microprobe (EMPA) and laser-ablation inductively-coupled plasma mass spectrometry (LA-ICP-MS) for major (including F, Rb) and trace (Li, Sc, Ga, Ge, Nb, In, Sn, Cs, Ta, Tl, W) elements, respectively. All primary micas at Cínovec are trioctahedral Li-Fe micas close to the annite–zinnwaldite–trilithionite series. Biotite from granites in the deeper part of the pluton (depth of 735–1596 m) contains 33.9–39.6 wt% SiO_2, 19.6–23.8 wt% FeO, 0.5–0.7 wt% Rb_2O, 0.9–1.8 wt% Li_2O, 3.4–4.8 wt% F, 381–937 ppm Nb, 34–134 ppm Ta, 20–46 ppm W, and 93–617 ppm Sn. Zinnwaldite from granites in the upper part of the pluton (depth of 0–735 m) contains 41.2–48.5 wt% SiO_2, 8.9–15.2 wt% FeO, 0.9–1.9 wt% MnO, 2.0–4.4 wt% Li_2O, 0.8–1.9 wt% Rb_2O, 7.0–8.6 wt% F, 43–464 ppm Nb, 101–213 ppm Sn, 6–80 ppm Ta, and 28–52 ppm W. Zinnwaldite from bodies of pervasive greisen and quartz-zinnwaldite veins is, compared to zinnwaldite from granites, relatively slightly enriched in Si, Mn and Ga, and depleted in Fe, F, Rb, Sn, W and Nb; Li and Ta contents are similar. Contents of Li, Rb and F, and the Fe/Mn and Nb/Ta values in mica closely positively correlate with those in the bulk rock, illustrating an upwards fractionation of parental melt. In contrast, the contents of high-field-strength elements in mica do not correspond to their contents in the bulk rock (melt): they were controlled by the order of crystallization of mica *vs.* accessory oxide minerals. Therefore, biotite generally contains distinctly higher Sn, Nb, Ta, and W than zinnwaldite. Dioctahedral micas of the muscovite–phengite series were found only as a late product of alteration of primary trioctahedral mica. Replacement of greisen-stage zinnwaldite by muscovite is chemically expressed in a strong depletion in Fe, F, and Li, and an enrichment in Sn. The share of trioctahedral mica in the bulk-rock budget of Sn decreases from 40–70% in biotite granite to less than 5% in greisen; in the case of Nb and Ta from 20–50% to less than 10%. The share of mica in the budget of W, mostly in the range of 2–15%, is stable through the whole pluton.

1. Introduction

Micas are chemically the most variable mineral group among all rock-forming minerals. Due to their specific layered crystal structure, micas are able to accommodate relatively high contents of many minor and trace elements (Bailey, 1984; Wise, 1995; Xie et al., 2015; Li et al., 2015). Chemical composition of magmatic micas, such as an enrichment in lithophile elements (Li, Rb and F), may indicate chemical composition of parental melt (Černý et al., 1985; Monier et al., 1987; Roda et al., 1995; Roda-Robles et al., 2012). To the contrary, micas easily equilibrate with hydrothermal fluids, changing their major- and trace-element compositions considerably (Van Lichtervelde et al., 2008; Petrík et al., 2014). Nevertheless, a careful evaluation of mica chemistry may help in the interpretation of the evolution of complex granitic plutons and associated mineral deposits (Brigatti et al., 2000; Van Lichtervelde et al., 2008; Johan et al., 2012; Legros et al., 2016).

The present work is aimed at proving the significance of Li-micas for the concentration of volatiles and trace elements during pronounced magmatic fractionation and following metasomatic greisenization. The well-known greisen-type Cínovec Li-Sn-W deposit in the eastern

* Corresponding author.
E-mail address: breiter@gli.cas.cz (K. Breiter).

https://doi.org/10.1016/j.oregeorev.2019.01.013
Received 18 May 2018; Received in revised form 4 January 2019; Accepted 10 January 2019
Available online 19 January 2019
0169-1368/

Erzgebirge was chosen as a typical object for this purpose, including the 1.6 km deep borehole CS-1 in its center.

First data on the chemical composition of mica from the Li-Sn-W Cínovec deposit were published by Johan et al. (2012) and later in a comprehensive study on granitic micas from the Bohemian Massif (Breiter et al., 2017b). The data set was now complemented with a detailed study of mica from the mineralized parts of the granite cupola. All data will be treated from three main points: (i) to decipher the vertical zoning of mica composition through an ore-bearing granite pluton, (ii) to check differences in the composition between magmatic and hydrothermal (greisen-stage) mica, and (iii) to evaluate the share of mica in the budget of ore elements Sn, W, Nb, Ta, and Sc throughout the mineralized granite–greisen system.

2. Geological background and samples

The Cínovec rare-metal granite cupola is situated on both sides of the Czech–German state border in the eastern part of the Krušné Hory/Erzgebirge Mts. as the youngest evolutionary member of the late Variscan Altenberg-Teplice rhyolite caldera (Hoth et al., 1995; Breiter, 1997; Mlčoch and Skácelová, 2010; Walther et al., 2016).

The caldera is transected from NW to SE by mostly hidden subsurface ridge of A-type granites, with several local elevations rising to the present surface (Fig. 1). One of them is the Cínovec/Zinnwald (Czech and German synonyms) cupola with an exposure of 1.4 × 0.3 km. A specific feature of the rare-metal granites (RMGs) in the Erzgebirge is their intrusion to a subvolcanic level, as proved by the formation of explosive breccia pipes (Seltmann et al., 1987). From the viewpoint of geochemistry, the Cínovec pluton represents strongly fractionated A-type granite: it is only slightly peraluminous, enriched in F, Li, Rb, Zr, Th, HREE, Sc, Sn, W, Nb, and Ta, and depleted in P, Ti, Mg, and Ca (Breiter et al., 2017a).

The RMG plutons often show a distinct vertical stratification (e.g., Beskin et al., 1994; Raimbault et al., 1995; Yin et al. 1995; Syritso et al., 2001), with the Cínovec being an excellent example (Štemprok and Šulcek, 1969; Breiter et al., 2017a) (Fig. 2):

- A fine-grained, strongly porphyritic variety of zinnwaldite granite, locally known as zinnwaldite microgranite (ZiGm, Fig. 3a), forms a hem up to several tens of meters thick along the upper part of the cupola. It is composed of euhedral quartz and perthite and subhedral albite phenocrysts (up to 5–10 mm across), cemented by fine-grained (< 0.5 mm) matrix of the same composition. Macroscopically black poikilitic zinnwaldite is common; topaz, fluorite, zircon, rutile and thorite are accessory. This facies represents the first portion of melt, fast crystallized along the upper contact of the intrusion. This carapace granite was partially destructed shortly after crystallization, and large xenoliths plunged into underlying melt.
- The upper part of the cupola, the “canopy”, to a depth of 260 m is composed of mostly leucocratic equigranular fine-grained albite-zinnwaldite granite (ZiGC, Fig. 3b). The granite consists of albite, quartz, zinnwaldite and sericitized K-feldspar. Typical accessory minerals are fluorite, topaz, zircon, cassiterite and columbite.
- Banded quartz–zinnwaldite veins (QZV, ± topaz, K-feldspar, wolframite, cassiterite), form a well-known onion-like structure in the central part of the cupola. The veins 20–200 cm thick are rimmed by a cm- to m-sized selvage of quartz-zinnwaldite metasomatic greisen mineralized by cassiterite and scheelite. Steep quartz–zinnwaldite veins, striking SW–NE and texturally similar to the previous type, are rare.
- Bodies termed “massive greisen” by the miners (GR) are flat zones of pervasive metasomatic greisenization tens to hundreds meters in size; they were typically formed 20–200 m beneath the granite/rhyolite contact. The combination of predominantly irregular steep joints with flat L-shaped joints enabled fluid migration and intensive replacement of feldspars by quartz, zinnwaldite, topaz and fluorite. Mineralization is irregularly distributed in the greisens: cassiterite strongly prevails over scheelite.
- Mica-free granite (MfG) was encountered at a depth of 260–369 m as a medium-grained porphyritic rock composed of up to 10 mm-sized perthite phenocrysts in quartz–K-feldspar–albite groundmass. Zinnwaldite is present only incidentally. Fluorite, zircon, rutile, thorite, cassiterite and columbite are typical accessories. Potassium-dominated fine- to medium-grained feldspathites (FSP) form several layers up to 5 m thick within the MfG body.
- A zone of large xenoliths of ZiGm (Fig. 3a) with local mingling with the ZiG appears at a depth of 369–530 m.
- Medium- to coarse-grained albite-zinnwaldite granite (ZiG, Fig. 3c) at the depth of 530–740 m is almost white and is texturally and mineralogically homogeneous. It is composed of perthite, quartz, albite and macroscopically black zinnwaldite. The granite further comprises topaz, fluorite, zircon, xenotime, thorite, monazite, rutile, cassiterite, columbite, scheelite and pyrochlore.
- The suite of biotite granites at the depth of 735–1596 m is homogeneous in its mineral and chemical compositions but exhibits various textures. Slightly porphyritic medium-grained biotite granite prevails (BtG, Fig. 3d). A fine-grained, distinctly porphyritic facies (“biotite microgranite”, BtGm, Fig. 3e) is subordinate. The pink color of the rocks is characteristic. All textural varieties of BtG contain accessory amounts of zircon, xenotime, thorite, monazite and rutile.

Altogether 38 samples covering all granite and greisen facies in a vertical section of the pluton to the depth of 1.6 km were collected (Table 1). Polished thin slabs 250–300 μm thick were prepared from all samples. Bulk-rock chemical analyses of all samples were available from the previous stage of the deposit investigation (Breiter et al., 2017a), and the complete dataset is available as an electronic supplement to the aforementioned paper.

3. Methods

Major elements in micas were analyzed using a CAMECA SX100 electron microprobe housed in the Institute of Geology of the Czech Academy of Sciences, Praha. We used an accelerating voltage of 15 kV, a beam current of 10 nA, and a beam diameter of 2 μm. The following standards were used: Na, Al – jadeite, Mg, Si, Ca – diopside, K – leucite, Ti – rutile, P – apatite, Mn – $MnCr_2O_4$, Fe – magnetite, F – fluorite, Rb – RbCl. The counting times on each peak were optimized for individual elements according to their expected concentrations (10–60 s), and half that time was used to obtain background counts. X-ray lines and background offsets were selected to minimize interference. The X-Phi correction procedure (Merlet, 1994) was applied. Chemical analyses of micas were recalculated to the proposed structural formulae based on 44 negative charges.

The trace elements in the micas were analyzed at the Laboratory of Atomic Spectrochemistry (LAS), Department of Chemistry, Faculty of Science, Masaryk University Brno. Besides Li, we decided to analyze another 10 elements: Sn, W, Nb and Ta as rare metals which are enriched and potentially mineable at the deposit, Cs and Tl as rare elements geochemically similar to K and potentially concentrating in micas (Rb was already analyzed by the EMPA), Ga and Ge as potential indicators of magma fractionation (as decreasing Al/Ga and Si/Ge values, Argollo and Schilling, 1978; Breiter et al., 2013), and Sc and In as rare elements enriched at mineral deposits across the eastern Erzgebirge (Seifert and Sandmann, 2006; Kempe and Wolf, 2006). A pulsed Nd:YAG-based laser ablation system UP 213 (New Wave Research, Inc., Fremont, CA, USA) operating at 213 nm and equipped with a SuperCell was used for sampling. The ablation-generated aerosol was transported using helium carrier gas (1 l min^{-1}) into the ICP source of the quadrupole-based mass spectrometer Agilent 7500ce (Agilent Technologies,

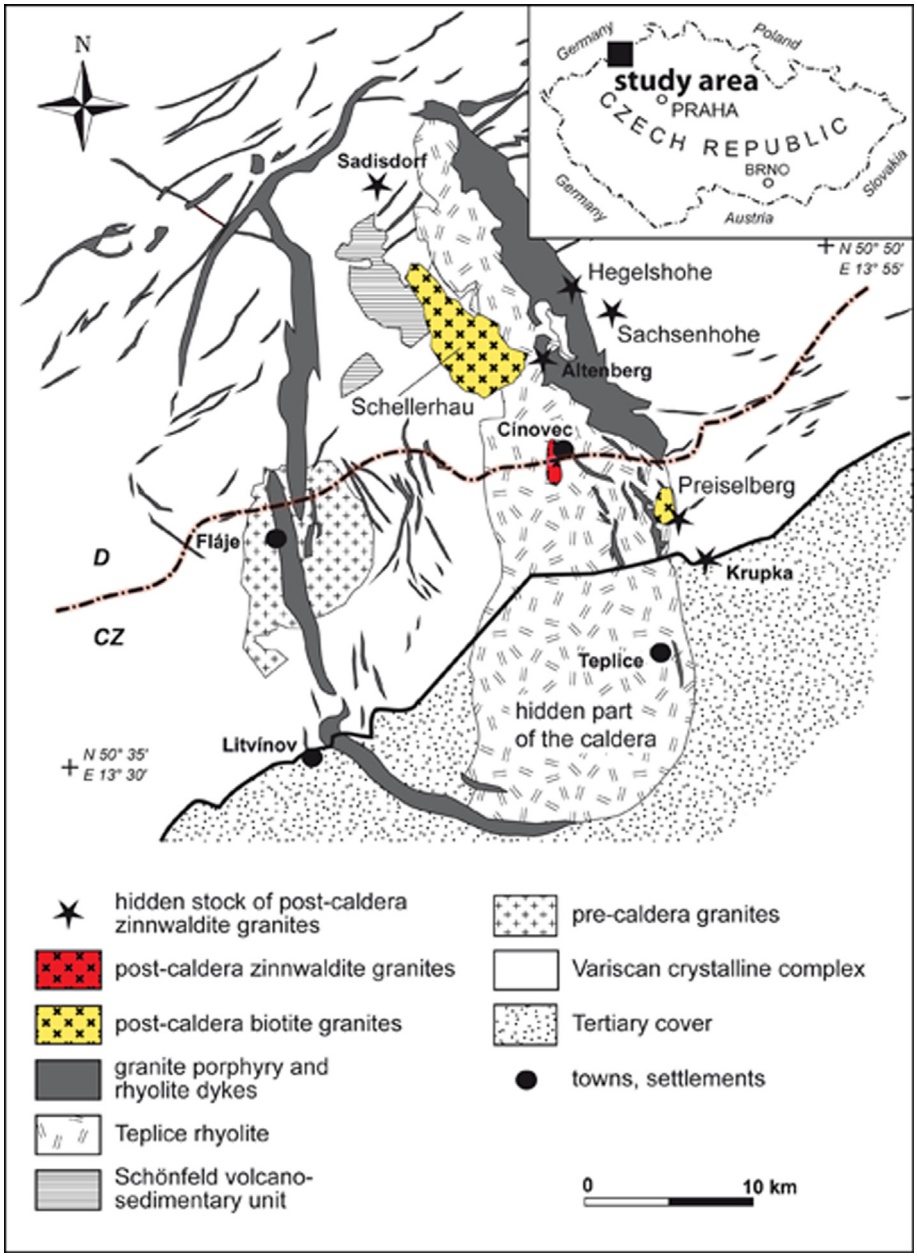

Fig. 1. Simplified geological map of the Altenberg-Teplice caldera. Modified according to Hoth et al. (1995) and Mlčoch and Skácelová (2010).

Santa Clara, CA, USA). The He carrier gas was mixed with argon make-up gas *via* a Y-connector prior to the ICP. To minimize potential polyatomic interferences, a collision-reaction cell in He mode (1 ml min^{-1}) was used. Time-resolved signals for the following isotopes were recorded: $^{7}Li^{+}$, $^{27}Al^{+}$ and $^{28}Si^{+}$ as matrix elements, and $^{45}Sc^{+}$, $^{69}Ga^{+}$, $^{72}Ge^{+}$, $^{93}Nb^{+}$, $^{115}In^{+}$, $^{118}Sn^{+}$, $^{133}Cs^{+}$, $^{181}Ta^{+}$, $^{182}W^{+}$ and $^{205}Tl^{+}$ as trace elements. An integration time of 0.1 s was used except for Ge (0.5 s) and In (0.7 s). A fluence of 13 J cm^{-2} was found to be optimal, and a spot diameter of 50 µm and a repetition rate of 10 Hz were fixed. Each spot analysis incorporates approximately 30 s of background (Ar-He gas blank) followed by 40 s of data acquisition from the sample. Contents were calculated from the background-corrected peak areas using NIST SRM 612 and NIST SRM 610 and Si as the internal reference element. The detection limits were calculated as three times the standard deviation of the background divided by the sensitivity (defined as the isotope intensity to elemental content ratio). The average detection limits under the operating conditions were as follows: 1.8 ppm Li; 1.5 ppm Al; 170 ppm Si; 0.70 ppm Sc; 0.18 ppm Ga; 1.0 ppm Ge; 0.08 ppm Nb; 0.04 ppm In; 2.1 ppm Sn; 0.15 ppm Cs; 0.08 ppm Ta; 0.21 ppm W and 0.41 ppm Tl.

To calculate the share of mica in the budget of rare metals in the bulk rock (Fig. 11), modal contents of mica in the rock sample should be determined with the highest possible precision. While mica is the only host of Li in the studied rocks, modal contents of mica in rock samples were calculated based on the bulk-rock Li contents (data published in Breiter et al., 2017a) and Li contents in the particular mica analyzed by LA-ICP-MS.

4. Terminological remark

According to the IMA rules, only so-called “end member” mineral names are valid. Actual nomenclature of micas (Rieder et al., 1999) is based on this rule. Nevertheless, in the case of rock-forming minerals important for igneous rock classification, practical petrology typically uses more detailed mineral classifications. In this paper, therefore, we use the traditional name zinnwaldite (Haidinger, 1845; Rieder et al.,

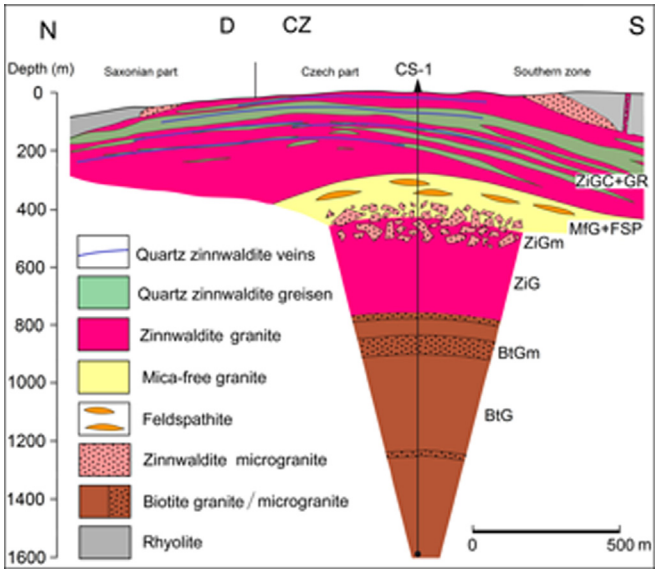

Fig. 2. A cross-section through the Cínovec granite pluton and greisen deposit (according to Breiter et al., 2017a, modified).

1996) for Li-rich micas that are close to the intersection of the siderophyllite–polylithionite and the annite–trilithionite join with preferred formula $K_2Li_2Fe_2Al_2(Al_2Si_6O_{20})F_4$. Micas close to this composition are common not only in the granites and greisens at Cínovec, but also in Sn- and W-bearing granites worldwide (Stone et al., 1988; du Bray, 1994). In the older literature, also the name protolithionite has been used for mica from deeper parts of the Cínovec cupola (Štemprok and Šulcek, 1969; Johan et al., 2012). Protolithionite (sensu Weiss et al., 1993) with preferred formula $K_2LiFe_4Al(Al_2Si_6O_{20})$ (F, $OH)_4$ situated on the zinnwaldite–annite join is common in relatively less evolved facies of rare-metal granite systems. Nevertheless, the usage of this name was not recommended by IMA (Rieder et al., 1999).

For simplicity, this paper adheres to the name "zinnwaldite" for micas containing more than 1.2 apfu Li, and the name "biotite" for the Li-poorer micas (Fig. 4). Such classification is in accord with geological structure of the Cínovec pluton, composed of the deeper intrusion of "biotite granite" and the upper intrusion of "zinnwaldite granite" including greisen bodies and quartz-zinnwaldite veins. This simplified classification is also corroborated by two styles in Li substitution mechanism in mica crystal lattice (Breiter et al., 2017b).

5. Results

We studied micas in polished slabs from 38 granite and greisen samples. Typical shapes of mica grains are shown in Figs. 5 and 6.

Zinnwaldite from the middle part of the cupola (ZiG, ZiGm) is macroscopically black (Figs. 3a, c, 5a), forming grains 2–5 mm in size with numerous inclusions of fluorite, zircon, monazite, xenotime and Nb,Ta-enriched rutile. Zinnwaldite from the uppermost part of the cupola is silvery (in greisen, Fig. 5b) or light-brown to colorless (disseminated in granite, Figs. 3b, 5c). In veins, monomineral bands up to 5 cm thick and several m^2 in size with individual flakes larger than 10 cm^2 are common. This zinnwaldite is poor in mineral inclusions (Fig. 5b, c). Local muscovitization of zinnwaldite was encountered in some greisen bodies (Fig. 6). The contents of zinnwaldite in ZiG and ZiGm are about 5 vol%, decreasing to 2 vol% in albite-rich ZiGC, but increasing up to 40 vol% in greisens. Late muscovitization, locally developed in greisen bodies, is connected with the post-greisen Sn-transfer and will be discussed later.

Macroscopically black biotite constitutes 2–4 vol% of biotite

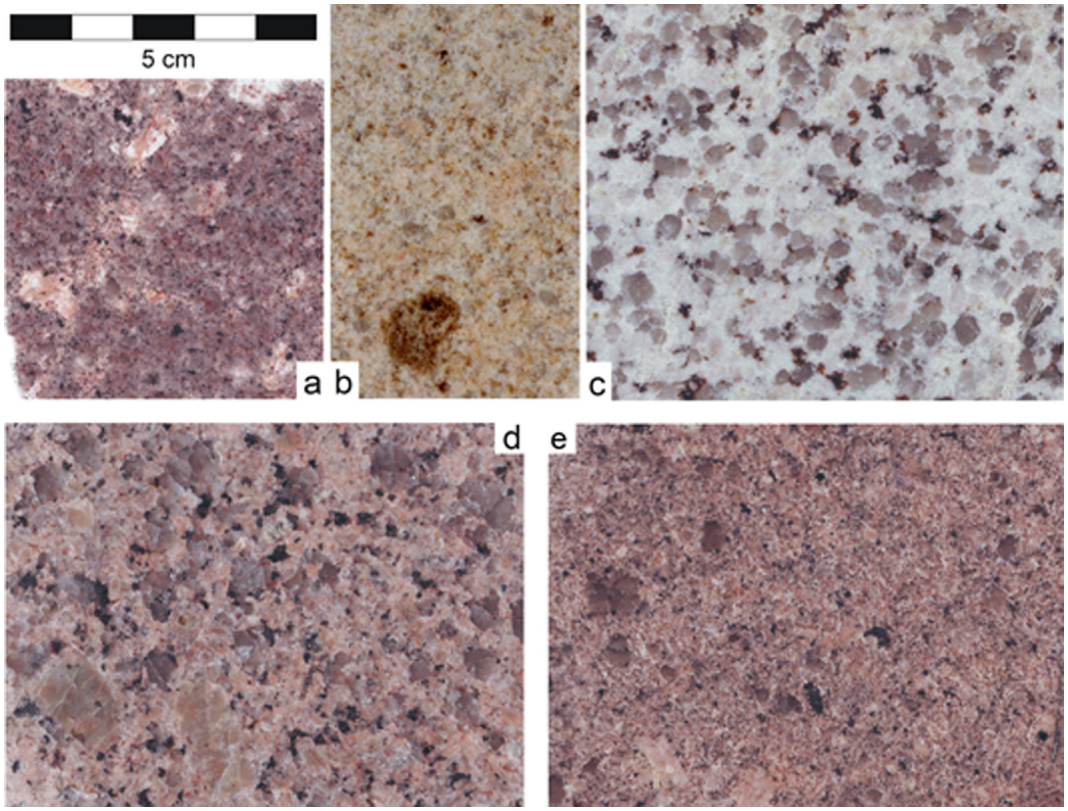

Fig. 3. Macroscopic photographs of typical granites from the Cínovec cupola: a, zinnwaldite microgranite with black zinnwaldite (a xenolith, CS-1, depth 413 m); b, zinnwaldite granite of the upper part of the cupola with light brown zinnwaldite (CS-1, depth 87 m); c, zinnwaldite granite from the middle part of the cupola with black zinnwaldite (CS-1, 608 m); d, biotite granite (CS-1, depth 1400 m); e, biotite microgranite (CS-1, depth 914 m).

Table 1
List of analyzed samples.

Sample	Borehole	Depth (m)	Rock type	Symbol	Description
4970	CS-1	35	quartz-zinnwaldite vein	QZV	thin flat quartz-zinnwaldite vein with greisen selvages
4674	CS-1	40	zinnwaldite granite	ZiGC	fine-grained albite-zinnwaldite leucogranite with strong sericitization of Kfs
4683	CS-1	97	zinnwaldite granite	ZiGC	medium-grained zinnwaldite leucogranite
4971	CS-1	130	quartz-zinnwaldite vein	QZV	thin flat quartz-zinnwaldite vein in granite
4972A	CS-1	149	greisen	GR	quartz-zinnwaldite greisen with miaroles and with selective muscovitization of rims of the zinnwaldite flakes, mica-rich part
4972B	CS-1	149	greisen	GR	quartz-zinnwaldite greisen with miaroles and with selective muscovitization of rims of the zinnwaldite flakes, quartz-rich part
4973	CS-1	163	greisen	GR	quartz-zinnwaldite greisen with miaroles filled by clay minerals
5048	CS-1	182	zinnwaldite granite	ZiGC	altered medium-grained zinnwaldite granite
4974	CS-1	193	greisen	GR	quartz-zinnwaldite greisen
4685	CS-1	205	zinnwaldite granite	ZiGC	medium-grained zinnwaldite granite with strongly sericitized feldspars
4975	CS-1	213	zinnwaldite granite	ZiGC	slightly greisenized zinnwaldite granite
5064	CS-1	244	zinnwaldite granite	ZiGC	medium-grained zinnwaldite granite
4687	CS-1	413	zinnwaldite microgranite	ZiGm	fine-grained porphyritic zinnwaldite granite
4936	CS-1	477	zinnwaldite microgranite	ZiGm	fine-grained porphyritic zinnwaldite granite
4688	CS-1	559	zinnwaldite granite	ZiG	medium-grained zinnwaldite granite, fresh
4938	CS-1	653	zinnwaldite granite	ZiG	medium-grained zinnwaldite granite, fresh
4689	CS-1	735	zinnwaldite granite	ZiG	medium-grained zinnwaldite granite, fresh
4690	CS-1	741	biotite microgranite	BtGm	fine-grained strongly porphyritic biotite granite
4691	CS-1	749	biotite granite	BtG	fine- to medium-grained porphyritic granite
4801	CS-1	774	biotite granite	BtG	medium-grained porphyritic biotite granite
5171	CS-1	800	biotite granite	BtG	medium-grained porphyritic biotite granite
4802	CS-1	860	biotite microgranite	BtGm	fine-grained strongly porphyritic biotite granite
4692	CS-1	988	biotite granite	BtG	medium-grained porphyritic biotite granite
4940	CS-1	1025	biotite granite	BtG	medium-grained porphyritic biotite granite
4941	CS-1	1245	biotite microgranite	BtGm	fine-grained strongly porphyritic biotite granite
4942	CS-1	1400	biotite microgranite	BtGm	fine-grained strongly porphyritic biotite granite
4693	CS-1	1579	biotite granite	BtG	medium-grained porphyritic biotite granite
5423	Cis-2	180	zinnwaldite granite	ZiGC	fine-grained fine-porphyritic zinnwaldite granite
5425	Cis-2	186	zinnwaldite granite	ZiGC	fine-grained equigranular zinnwaldite granite
5427	Cis-2	190	greisen	GR	zinnwaldite-rich greisen
5428	Cis-2	191	greisen	GR	quartz-zinnwaldite greisen
5429	Cis-2	280	zinnwaldite granite	ZiGC	altered medium-grained zinnwaldite granite
5430	Cis-2	374	zinnwaldite granite	ZiGC	altered medium-grained zinnwaldite granite
5438	PSn07	332	greisen	GR	quartz-rich greisen with zinnwaldite
5436	PSn07	343	zinnwaldite granite	ZiGC	medium-grained zinnwaldite granite
5434	PSn07	412	zinnwaldite granite	ZiGC	medium-grained granite with scarce zinnwaldite
4981	Bunau Stollen		greisen	GR	quartz-rich greisen with zinnwaldite
5412	Bunau Stollen		quartz-zinnwaldite vein	QZV	flat quartz vein with zinnwaldite rims

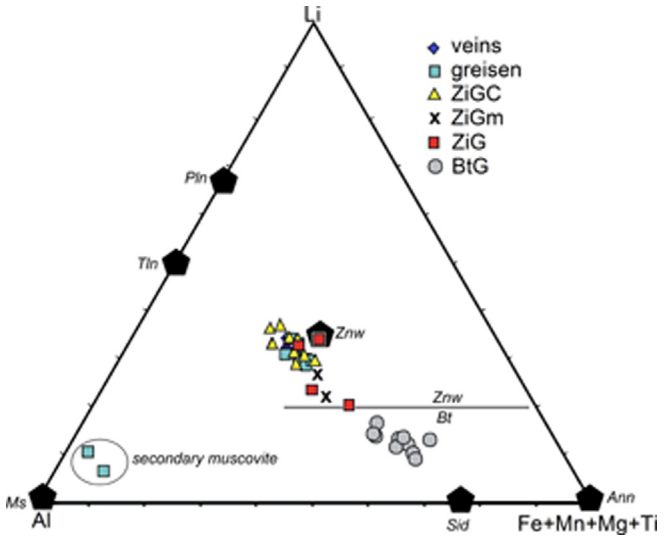

Fig. 4. Classification of Li-micas according to Foster (1960) showing the occupancy of the hexahedral site in coordinates Li–Fe + Mn + Mg + Ti–Al. Ideal IMA endmembers: Ann – annite, Sid – siderophyllite, Ms – muscovite, Znw – zinnwaldite, Tln – trilithionite, Pln – polylithionite. Empirical discrimination between biotite and zinnwaldite from Cínovec at Li = 1.2 apfu is shown. Figurative points near the muscovite apex represent a product of late muscovitization of greisen zinnwaldite (compare also with Fig. 6).

granites. Individual subhedral to anhedral flakes, mostly 0.5–2 mm across, often contain common inclusions of monazite, xenotime, zircon and Ti-oxides, sometimes associated with fluorite (Fig. 5d, e). Only a slight chloritization was encountered in some biotite grains from the deeper part of the cupola (depth of 1000–1596 m, Fig. 5f); this late style of alteration was not studied in detail. From each rock sample, 4–6 mica grains with 2 EMPA spots (core and rim) and 4–5 LA spots were analyzed, e.g., 8–12 EMPA and 15–25 LA spots in each sample in average. After elimination of ca. 10% of outliers (mainly occasional hits of mineral inclusions or cleavage), the primary database contains 364 EMPA and 814 LA spot analyses. The data presented in the tables represent average values of major elements (Table 2), structural formulae (Table 3) and medians and median absolute deviations of trace elements (Table 4) of all samples.

All primary micas at Cínovec are trioctahedral Li-Fe micas close to the annite–zinnwaldite–trilithionite series (Fig. 4). Dioctahedral micas of the muscovite–phengite series were found only as late products of alteration of primary trioctahedral micas, and as very fine-grained late alterations of K-feldspar (sericite).

With respect to major elements including Li, Rb and F, the trioctahedral micas can be classified into two distinct groups: zinnwaldite and Li-enriched biotite. Zinnwaldite contains 41.2–48.5 wt% SiO_2, 8.9–15.2 wt% FeO, 0.9–1.9 wt% MnO, 2.0–4.4 wt% Li_2O, 0.8–1.9 wt% Rb_2O and 7.0–8.6 wt% F. The contents of TiO_2 and MgO are very low, usually less than 0.3 and 0.1 wt%, respectively. In contrast, biotite contains 33.9–39.6 wt% SiO_2, 19.6–23.8 wt% FeO, 0.4–1.2 wt% MgO, 0.5–1.4 wt% TiO_2, 0.5–0.7 wt% MnO, 0.5–0.7 wt% Rb_2O, 0.9–1.8 wt%

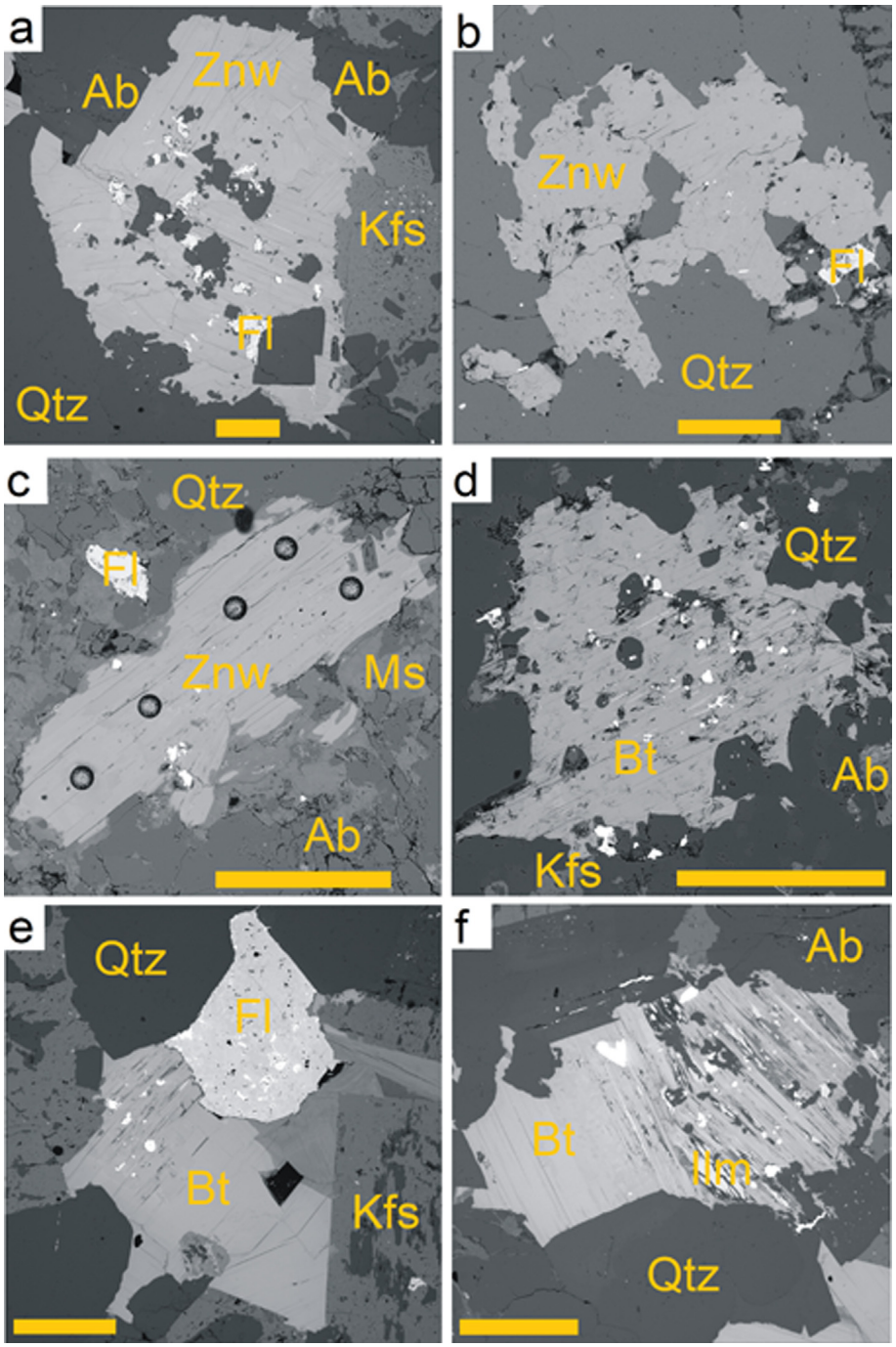

Fig. 5. Back-scattered electron (BSE) images of typical mica grains: a: mica from the deeper part of the albite-zinnwaldite granite (#4689, borehole CS-1, depth of 735 m), 2.02 wt% Li_2O (on the zinnwaldite–protolithionite join), typically contains inclusions of quartz and fluorite and small inclusions of zircon, monazite, xenotime and thorite; b: mica from the quartz-zinnwaldite greisen (#4974, borehole CS-1, depth of 193 m) with 3.43 wt% Li_2O, near "ideal" zinnwaldite; c: mica from the albite-zinnwaldite granite in the uppermost part of the cupola (#4674, borehole CS-1, depth of 40 m) with 4.20 wt% Li_2O (on the zinnwaldite–trilithionite join), laser-ablations spots 50 μm in diameter are visible; d: mica from biotite microgranite (#4690, borehole CS-1, depth of 741 m), contains 1.80 wt% Li_2O, near ideal protolithionite with inclusions of quartz and small inclusions of zircon and thorite; e: mica from medium-grained porphyritic biotite granite (#4692, borehole CS-1, depth of 988 m), contains 1.10 wt% Li_2O, positioned on the protolithionite–annite join; in association with a large grain of fluorite f: slightly chloritized mica from coarse-grained biotite granite (#4693, borehole CS-1, depth of 1579 m), contains 1.49 wt% Li_2O, positioned on the protolithionite–annite join. Scale bars in all cases equal to 500 μm. Mineral abbreviations: Qtz – quartz; Ab – albite; Kfs – K-feldspar; Znw – zinnwaldite; Ms – muscovite; Bt – biotite; Fl – fluorite; Ilm – ilmenite.

Li_2O and 3.4–4.8 wt% F. The contents of Al_2O_3, K_2O and Na_2O are homogeneous in all mica types, attaining 18.7–21.2 wt%, 9.1–10.3 wt% and 0.2–0.3 wt%, respectively. The distribution of trace elements is more complicated, varying across broad intervals not only within a distinct mica type, but also within particular sample and grain. Nevertheless, no systematic differences between cores and rims were found.

Within the group of zinnwaldite, noticeable difference was found between samples from different facies of granite and greisen. For example, the contents of Nb decrease from 158–464 ppm in zinnwaldite from the lower part of the cupola (ZiG) to 45–91 ppm in zinnwaldite from the upper part of the cupola (ZiGC) and 36–70 ppm in zinnwaldite from greisen and veins. Similarly, Ta decreases from 80 ppm in zinnwaldite from the ZiG to 6–28 ppm in zinnwaldites from greisens and the ZiGC. The contents of Sn are scattered mostly between 100 and 200 (occasionally up to 530) ppm in zinnwaldite from the ZiG and 65–155 ppm in zinnwaldite from greisens, with no clear vertical trend. The contents of W are slightly higher in zinnwaldite from granites (28–74 ppm) than in zinnwaldite from greisen (13–39 ppm, in one sample only 2.9 ppm). Also the contents of Cs are slightly higher in zinnwaldite from granites (370–630 ppm) than in zinnwaldite from greisen (360–500 ppm). The contents of other analyzed trace elements in zinnwaldite from both rock types are similar: 42–100 ppm Sc, 32–55 ppm Tl, 66–160 ppm Ga, mostly 2.7–8 ppm Ge (in one case 14.5 ppm Ge) and mostly < 1 ppm In (occasionally up to1.4 ppm In).

In comparison with zinnwaldite, biotite from all facies of the BtG contains generally higher Nb (381–937 ppm), Ta (34–134 ppm), and Sn (93–617 ppm), while the contents of Cs (356–655 ppm), Sc (51–130 ppm), Ga (84–128 ppm), Ge (mostly 5.5–9.2 ppm) and In (mostly < 1 ppm) are similar. The contents of W (20–46 ppm) and Tl

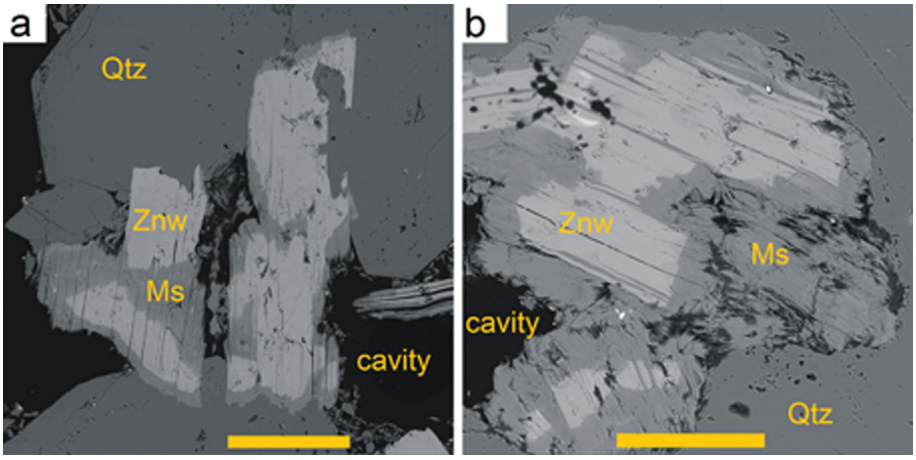

Fig. 6. Back-scattered electron (BSE) images of muscovitized micas: a: muscovitized zinnwaldite from zinnwaldite-rich greisen (#4972A, borehole CS-1, depth of 149 m); b: muscovitized zinnwaldite from quartz-rich greisen (#4972B, borehole CS-1, depth of 149 m). Scale bars 200 μm. Mineral abbreviations as in Fig. 5.

Table 2
Chemical composition (means) of micas (wt%). Li_2O analyzed via LA-ICP-MS, other via microprobe. Content of water computed on the basis of full occupation of the (F, OH) site (compare Table 3). For rock symbols see Table 1. Symbol "O = F" means the oxygen equivalent of fluorine.

Sample	Location	Depth (m)	Rock symbol	Mica	n	SiO_2	TiO_2	Al_2O_3	FeO	MnO	MgO	Rb_2O	Li_2O	Na_2O	K_2O	F	H_2O	O = F	Total
4970	CS-1	35	QZV	Znw	8	46.74	0.03	20.10	11.32	1.42	0.01	1.02	3.69	0.18	10.22	8.45	0.20	−3.56	99.82
4674	CS-1	40	ZiGC	Znw	14	47.80	0.13	19.78	8.91	1.33	0.03	1.86	4.20	0.23	9.89	8.56	0.17	−3.61	99.29
4683	CS-1	97	ZiGC	Znw	12	47.88	0.01	19.31	10.05	1.26	0.02	1.23	4.39	0.17	10.04	8.10	0.39	−3.42	99.43
4971	CS-1	130	QZV	Znw	8	46.07	0.15	20.02	11.97	1.22	0.02	1.11	4.01	0.19	9.74	8.07	0.36	−3.41	99.54
4972A	CS-1	149	GR	Znw	7	46.33	0.03	19.53	12.72	1.01	0.03	1.17	3.90	0.18	9.72	6.92	0.90	−2.91	99.54
4972A	CS-1	149	GR	Ms	7	48.63	0.00	31.31	2.08	1.05	0.09	0.39	0.60	0.03	10.08	0.88	4.03	−0.37	98.81
4972B	CS-1	149	GR	Znw	7	46.13	0.03	20.08	13.21	0.96	0.02	1.23	3.51	0.17	9.82	7.07	0.83	−2.98	100.09
4972B	CS-1	149	GR	Ms	5	48.33	< 0.01	34.34	1.17	0.14	0.09	0.26	1.02	0.05	10.02	0.41	4.36	−0.17	100.03
4973	Cs-1	163	GR	Znw	12	45.72	0.03	20.17	13.54	1.01	0.03	1.22	3.81	0.18	9.97	8.14	0.63	−3.43	101.02
5048	CS-1	182	ZiGC	Znw	7	45.93	0.22	19.89	12.53	0.91	0.09	1.36	3.79	0.23	9.58	7.95	0.41	−3.35	99.55
4974	CS-1	193	GR	Znw	8	45.17	0.18	20.39	13.91	0.93	0.04	1.89	3.43	0.23	9.69	8.12	0.32	−3.42	100.89
4685	CS-1	205	ZiGC	Znw	6	45.60	0.07	19.63	12.54	0.77	0.02	1.01	3.59	0.22	10.14	7.64	0.50	−3.22	98.52
4975	CS-1	213	ZiGC	Znw	8	45.46	0.24	20.39	13.00	0.81	0.10	0.98	3.25	0.23	9.72	8.01	0.35	−3.38	99.17
5064	CS-1	244	ZiGC	Znw	8	45.90	0.23	20.22	12.64	0.70	0.11	1.48	4.05	0.26	9.59	8.32	0.26	−3.51	100.25
4687	CS-1	413	ZiGm	Znw	12	42.88	0.53	20.64	16.38	0.77	0.18	0.82	2.42	0.23	9.79	6.94	0.78	−2.93	99.43
4936	CS-1	477	ZiGm	Znw	10	43.99	0.41	20.85	15.24	0.70	0.10	0.91	3.02	0.23	9.69	7.84	0.42	−3.30	100.10
4688	CS-1	559	ZiG	Znw	6	45.88	0.22	20.22	12.84	0.82	0.07	1.35	3.86	0.23	9.84	7.93	0.44	−3.35	100.36
4938	CS-1	653	ZiG	Znw	8	43.30	0.32	20.89	15.01	0.71	0.09	1.12	2.53	0.32	9.60	8.17	0.19	−3.44	98.81
4689	CS-1	735	ZiG	Znw	4	41.21	0.42	20.32	18.70	0.66	0.14	0.83	2.02	0.26	9.82	6.08	1.10	−2.56	99.00
4690	CS-1	741	BtGm	Bt	28	39.56	1.06	21.02	21.18	0.66	0.42	0.73	1.81	0.31	9.25	4.35	1.94	−1.83	100.46
4691	CS-1	749	BtG	Bt	4	39.58	0.75	19.93	20.11	0.59	0.70	0.71	1.41	0.29	9.64	3.78	2.11	−1.59	98.01
4801	CS-1	774	BtG	Bt	6	37.77	1.32	20.85	22.08	0.52	0.93	0.55	1.41	0.32	9.64	3.54	2.25	−1.49	99.70
5171	CS-1	800	BtG	Bt	12	37.80	1.37	19.98	22.66	0.50	1.00	0.49	1.26	0.31	9.29	4.72	1.65	−2.00	99.04
4802	CS-1	860	BtGm	Bt	6	37.93	1.21	20.46	22.43	0.57	0.44	0.62	1.19	0.30	9.59	3.44	2.26	−1.45	99.00
4692	CS-1	988	BtG	Bt	14	37.92	0.92	20.02	23.10	0.60	1.29	0.47	1.10	0.31	9.48	4.72	1.66	−1.99	99.61
4940	CS-1	1025	BtG	Bt	6	36.93	1.33	19.34	23.84	0.64	0.80	0.51	1.35	0.28	9.14	4.31	1.79	−1.81	98.45
4941	CS-1	1245	BtGm	Bt	9	37.40	1.20	19.88	23.78	0.64	0.72	0.50	0.94	0.28	9.35	4.22	1.86	−1.78	98.99
4942	CS-1	1400	BtGm	Bt	10	39.21	1.45	20.02	21.93	0.57	1.25	0.52	1.47	0.27	9.34	4.84	1.68	−2.04	100.52
4693	CS-1	1579	BtG	Bt	4	39.57	0.50	19.93	19.64	0.75	0.88	0.49	1.49	0.29	9.77	3.93	2.04	−1.65	97.64
5423	Cis-2	180	ZiGC	Znw	8	48.42	0.08	19.06	8.96	1.92	0.02	2.22	3.67	0.21	9.65	8.45	0.20	−3.56	99.30
5425	Cis-2	186	ZiGC	Znw	10	48.52	0.07	19.42	9.61	1.43	0.02	2.24	3.73	0.24	9.70	8.48	0.22	−3.58	100.10
5427	Cis-2	190	GR	Znw	3	45.92	0.03	18.69	13.27	1.38	0.01	1.07	3.13	0.23	10.12	7.83	0.39	−3.30	98.77
5428	Cis-2	191	GR	Znw	6	46.28	0.01	18.15	13.60	1.42	< 0.01	0.98	3.31	0.16	10.33	7.87	0.38	−3.32	99.18
5429	Cis-2	280	ZiGC	Znw	14	44.97	0.12	20.35	13.65	1.02	0.01	2.14	3.54	0.19	9.63	7.98	0.37	−3.37	100.60
5430	Cis-2	374	ZiGC	Znw	10	44.84	0.14	20.20	14.98	1.01	0.02	1.13	3.45	0.23	9.66	8.00	0.37	−3.37	100.66
5438	PSn07	332	GR	Znw	10	47.56	0.07	19.09	11.50	1.14	0.01	1.19	3.97	0.21	10.13	7.29	0.76	−3.07	99.85
5434	PSn07	412	ZiGC	Znw	12	46.52	0.20	19.72	12.47	0.78	0.07	1.31	3.58	0.25	10.13	7.16	0.80	−3.01	99.98
5436	PSn07	343	ZiGC	Znw	10	47.57	0.11	19.37	11.71	0.89	0.02	1.54	4.01	0.23	10.06	7.34	0.75	−3.09	100.51
4981	Bunau Stollen		GR	Znw	8	47.29	0.01	19.49	11.46	1.24	0.01	1.07	3.45	0.19	10.16	8.48	0.17	−3.57	99.46
5412	Bunau Stollen		QZV	Znw	10	47.97	0.02	19.45	11.20	1.35	0.01	0.91	4.03	0.15	10.05	8.44	0.25	−3.56	100.27

(17–33 ppm) in biotite are lower than those in zinnwaldite. Along basic division of trioctahedral micas to zinnwaldite and biotite, systematic chemical changes in vertical direction along borehole CS-1are noticeable (Figs. 7, 8). The contents of major elements Si, Al, Fe, Li and F show a regular trend with principal change at the depth of 735 m, corresponding to the contact between biotite and zinnwaldite granites (Fig. 7). The contents of major elements are scattered within the BtG with no obvious trend but their systematic evolution within the intrusion of zinnwaldite granites corroborates the general petrological-geochemical trend of upwards fractionation (Breiter et al., 2017a): the contents of Fe and Al decrease, whereas the contents of Si, Li, Rb and F increase in upward direction. The most intensive variations can be seen

Table 3
Structural formulae of micas (apfu) on the basis of 44 negative charges.

Sample	Si	Al^{IV}	Total T	Ti	Al^{VI}	Fe	Mn	Mg	Li	Total Y	Na	K	Rb	Total Z	F	OH
4970	6.669	1.331	4	0.003	2.049	1.351	0.172	0.002	2.117	5.694	0.050	1.860	0.094	2.003	3.813	0.187
4674	6.786	1.214	4	0.014	2.095	1.058	0.160	0.006	2.398	5.731	0.063	1.791	0.170	2.024	3.843	0.157
4683	6.787	1.213	4	0.001	2.013	1.191	0.151	0.004	2.502	5.863	0.047	1.815	0.112	1.974	3.631	0.369
4971	6.596	1.404	4	0.016	1.974	1.433	0.148	0.004	2.309	5.884	0.053	1.779	0.102	1.934	3.653	0.347
4972A	6.646	1.354	4	0.003	1.947	1.526	0.123	0.006	2.250	5.855	0.050	1.779	0.108	1.936	3.139	0.861
4972A	6.557	1.443	4	0.000	3.532	0.235	0.120	0.018	0.325	4.229	0.008	1.734	0.034	1.775	0.375	3.625
4972B	6.608	1.392	4	0.003	1.998	1.582	0.116	0.004	2.022	5.726	0.047	1.794	0.113	1.955	3.202	0.798
4972B	6.360	1.640	4	0.000	3.686	0.129	0.016	0.018	0.540	4.387	0.013	1.682	0.022	1.717	0.171	3.829
4973	6.534	1.466	4	0.003	1.930	1.618	0.122	0.006	2.190	5.870	0.050	1.817	0.112	1.929	3.678	0.322
5048	6.598	1.402	4	0.024	1.966	1.505	0.111	0.019	2.190	5.815	0.064	1.756	0.126	1.945	3.612	0.388
4974	6.493	1.507	4	0.019	1.947	1.672	0.113	0.009	1.983	5.743	0.064	1.777	0.175	2.015	3.691	0.309
4685	6.626	1.374	4	0.008	1.987	1.524	0.095	0.004	2.098	5.715	0.062	1.879	0.094	2.036	3.510	0.490
4975	6.566	1.434	4	0.026	2.037	1.570	0.099	0.022	1.888	5.642	0.064	1.791	0.091	1.946	3.658	0.342
5064	6.548	1.452	4	0.025	1.948	1.508	0.085	0.023	2.324	5.912	0.072	1.745	0.136	1.953	3.753	0.247
4687	6.320	1.680	4	0.059	1.906	2.019	0.096	0.040	1.434	5.553	0.066	1.841	0.078	1.984	3.235	0.765
4936	6.379	1.621	4	0.045	1.943	1.848	0.086	0.022	1.761	5.704	0.065	1.792	0.085	1.942	3.595	0.405
4688	6.551	1.449	4	0.024	1.954	1.533	0.099	0.015	2.216	5.841	0.064	1.792	0.124	1.980	3.580	0.420
4938	6.386	1.614	4	0.035	2.016	1.851	0.089	0.020	1.500	5.512	0.091	1.806	0.106	2.004	3.810	0.190
4689	6.200	1.800	4	0.048	1.803	2.353	0.084	0.031	1.222	5.541	0.076	1.885	0.080	2.041	2.893	1.107
4690	5.927	2.073	4	0.119	1.638	2.653	0.084	0.094	1.091	5.679	0.090	1.768	0.070	1.928	2.061	1.939
4691	6.073	1.927	4	0.087	1.678	2.580	0.077	0.160	0.870	5.451	0.086	1.887	0.070	2.043	1.834	2.166
4801	5.764	2.236	4	0.151	1.514	2.818	0.067	0.212	0.865	5.628	0.095	1.877	0.054	2.025	1.708	2.292
5171	5.825	2.175	4	0.159	1.453	2.920	0.065	0.230	0.781	5.607	0.093	1.826	0.049	1.967	2.300	1.700
4802	5.846	2.154	4	0.140	1.562	2.890	0.074	0.101	0.738	5.505	0.090	1.885	0.061	2.036	1.676	2.324
4692	5.831	2.169	4	0.106	1.458	2.970	0.078	0.296	0.680	5.589	0.092	1.859	0.046	1.998	2.295	1.705
4940	5.775	2.225	4	0.156	1.338	3.117	0.085	0.186	0.849	5.732	0.085	1.823	0.051	1.959	2.131	1.869
4941	5.813	2.187	4	0.140	1.455	3.091	0.084	0.167	0.588	5.525	0.084	1.854	0.050	1.988	2.074	1.926
4942	5.907	2.093	4	0.164	1.462	2.763	0.073	0.281	0.891	5.633	0.079	1.795	0.050	1.924	2.306	1.694
4693	6.080	1.920	4	0.058	1.690	2.524	0.098	0.202	0.921	5.491	0.086	1.915	0.048	2.050	1.910	2.090
5423	6.906	1.094	4	0.009	2.109	1.069	0.232	0.004	2.105	5.528	0.058	1.756	0.203	2.017	3.811	0.189
5425	6.869	1.131	4	0.007	2.110	1.138	0.171	0.004	2.124	5.554	0.066	1.752	0.204	2.021	3.796	0.204
5427	6.712	1.288	4	0.003	1.931	1.622	0.171	0.002	1.840	5.569	0.065	1.887	0.100	2.052	3.619	0.381
5428	6.745	1.255	4	0.001	1.862	1.657	0.175	0.000	1.940	5.635	0.045	1.920	0.092	2.057	3.627	0.373
5429	6.487	1.513	4	0.013	1.946	1.646	0.125	0.002	2.053	5.786	0.053	1.772	0.198	2.023	3.640	0.360
5430	6.460	1.540	4	0.015	1.890	1.805	0.123	0.004	1.999	5.837	0.064	1.775	0.105	1.944	3.645	0.355
5438	6.768	1.232	4	0.007	1.970	1.368	0.137	0.002	2.272	5.757	0.058	1.839	0.109	2.006	3.280	0.720
5434	6.658	1.342	4	0.022	1.984	1.492	0.095	0.015	2.060	5.668	0.069	1.849	0.120	2.039	3.240	0.760
5436	6.738	1.262	4	0.012	1.971	1.387	0.107	0.004	2.284	5.765	0.063	1.818	0.140	2.021	3.288	0.712
4981	6.771	1.229	4	0.001	2.060	1.372	0.150	0.002	1.986	5.572	0.053	1.856	0.098	2.007	3.839	0.161
5412	6.773	1.227	4	0.002	2.009	1.322	0.161	0.002	2.288	5.785	0.041	1.810	0.083	1.934	3.768	0.232

in the case of Fe, Li and F contents. Systematic evolution of mica composition is disturbed only in the zone of xenoliths of ZiGm at a depth of 369–530 m: zinnwaldite within the ZiGm is chemically less evolved (1.43–1.75 apfu Li) than zinnwaldite from the surrounding medium-grained ZiG (2.32 and 2.44 apfu Li).

Different patterns were encountered in vertical distribution of rare metals in mica: the contents of Sn, Nb and Ta decrease strongly upward: 620 → 70 ppm Sn, 550 → 50 ppm Nb and 70 → 20 ppm Ta (Fig. 8a, b, c). Local enrichment disturbing this trend was found in the upper part of the BtG (depth of ca. 740–750 m) and in the ZiGm (depth of 413 m), in both cases in coincidence with some enrichment of Sn in the bulk-rock. In case of biotite from BtG, the enrichment may be explained by influence of fluids from neighboring ZiG, in case of zinnwaldite from ZiGm the lack of Ti-oxide minerals pushed all Sn to the mica.

In contrast, the contents of W vary only slightly between 20 and 70 ppm, showing no trend (Fig. 8d). The highest contents of Sc (80–130 ppm) were found in the upper part of the BtG at a depth of 740–1000 m (Fig. 8e). The contents of all mentioned trace elements in mica do not correlate with their contents in the bulk rock; the entry of particular element into mica crystal lattice was controlled in particular namely by the associated mineral assemblage, i.e., with saturation of Ti, Sn, W, Nb and Ta-bearing oxide minerals.

Thallium is the only trace element the contents of which systematically increase upwards with maxima in the range of 40–60 ppm in the uppermost part of the ZiG. The contents of Tl in mica correlate well with Tl contents in the bulk rock, with $Tl_{mica}/Tl_{rock} \sim 5$ (Fig. 8f).

Of the elemental ratios proposed as indicators of magma fractionation (Černý et al., 1985), the Nb/Ta values decrease upwards (7 → 2) with disturbances in the uppermost part of the BtG and in the ZiGm. The Nb/Ta values in the whole rock decrease in a similar way: from 6.5 in the BtG through 3.5 in the ZiG to 2.7 in greisen and 2.5 in the ZiGC (Fig. 8g). Similarly, the Fe/Mn values, stable within the BtG, decrease systematically upwards in the ZiG, showing a perfect coincidence between the mica values and bulk-rock values (Fig. 8h). Concordance in the evolution of Nb/Ta and Fe/Mn values in columbite and bulk rock (Breiter et al., 2017c) and in micas and bulk rock (this paper) indicates an intensive equilibration of the whole mineral assemblage during the late magmatic/hydrothermal stage.

Dioctahedral mica of the muscovite–phengite series was found only locally as a product of late alteration of zinnwaldite flakes. Muscovite contains ca. 47.5–49.0 wt% SiO_2, 30.6–35.2 wt% Al_2O_3, 0.9–2.1 wt% FeO, 0.1–1.5 wt% MnO, 0.3–0.4 wt% Rb_2O, less than 0.1 wt% TiO_2, MgO and Na_2O, 0.1–1.6 wt% Li_2O, and 0.3–1.0 wt% F. Chemical boundary between muscovite and zinnwaldite is sharp without any visible transition zone (Fig. 6). The contents of Sn increase from 27–300 ppm to 600–1500 ppm during muscovitization (Fig. 9), while the contents of other trace elements are scattered with no distinct trends.

6. Discussion

6.1. Reliability of Li computation from microprobe analyses (Fig. 10)

Lithium as the only major constituent of micas from evolved

Table 4
Contents of trace elements (medians and median absolute deviations) in micas (ppm) analyzed via LA-ICP-MS.

Sample	Rock		Li	Sc	Ga	Ge	Nb	In	Sn	Cs	Ta	W	Tl
Detection limit			1.8	0.7	0.18	1.0	0.08	0.04	2.1	0.15	0.08	0.21	0.41
4970	QZV	median	17,154	56	115	6.8	39	0.47	109	231	20	19	44
		MAD	335	6	9	0.8	12	0.08	31	39	5	6	2
4674	ZiGC	median	19,472	76	67	4.8	55	0.36	123	631	26	48	55
		MAD	1536	4	6	0.9	12	0.23	41	80	4	7	4
4683	ZiGC	median	20,390	49	75	2.6	45	1.19	112	350	6	28	35
		MAD	860	2	2	0.3	9	0.20	15	13	2	6	0
4971	QZV	median	18,637	84	76	6.4	70	0.61	114	423	34	39	39
		MAD	456	2	5	0.3	6	0.07	16	58	3	4	2
4972A-Zin	GR	median	18,752	65	96	5.6	42	0.45	103	180	10	15	39
		MAD	793	4	11	0.6	12	0.24	45	38	5	4	2
4972A-Ms	GR	median	2640	66	78	1.2	9	2.33	1165	192	7	2	46
		MAD	2311	2	7	0.1	1	1.21	208	11	1	1	5
4972B-Znw	GR	median	15,778	62	77	3.1	24	1.16	145	273	10	13	45
		MAD	54	10	0	0.0	2	0.04	30	54	1	6	3
4972B-Ms	GR	median	5282	85	62	2.1	37	3.56	1408	182	26	10	37
		MAD	2071	3	3	0.1	19	0.09	213	28	15	5	4
4973	GR	median	17,715	71	125	19.0	54	0.37	68	448	18	19	53
		MAD	1062	9	15	2.0	9	0.09	13	108	5	5	5
5048	GR	median	17,617	83	71	7.1	85	0.42	101	467	29	45	39
		MAD	525	2	6	0.5	25	0.08	19	63	6	6	6
4974	GR	median	15,920	79	66	6.7	69	0.43	79	362	29	29	32
		MAD	644	6	4	0.7	11	0.06	15	26	7	7	2
4685	ZiGC	median	16,660	69	69	2.8	98	1.03	149	435	34	33	33
		MAD	1253	4	3	1.1	9	0.16	19	54	5	4	1
4975	ZiGC	median	15,084	81	70	13.1	41	0.77	80	399	14	18	35
		MAD	366	5	2	1.5	13	0.06	13	40	4	6	1
5064	ZiGC	median	18,817	86	82	6.7	91	0.31	118	472	22	40	42
		MAD	449	2	16	0.5	20	0.07	30	72	10	10	8
4687	ZiGm	median	11,255	62	94	6.3	313	0.38	238	467	41	36	46
		MAD	287	4	6	0.5	99	0.04	37	30	10	2	2
4936	ZiGm	median	14,033	78	86	5.9	172	0.26	139	528	29	39	34
		MAD	401	3	7	0.3	59	0.05	13	43	6	5	2
4688	ZiG	median	17,909	67	87	2.8	119	0.89	150	449	41	52	46
		MAD	1290	13	14	2.2	34	0.12	26	159	9	4	4
4938	ZiG	median	11,751	62	73	4.6	158	0.22	106	322	26	36	35
		MAD	363	10	11	0.3	37	0.03	24	46	4	7	2
4689	ZiG	median	9405	100	109	14.5	464	1.43	213	981	80	37	33
		MAD	809	12	5	1.3	155	0.20	28	158	6	9	2
4690	BtG	median	8406	83	104	6.5	631	2.22	444	400	41	46	33
		MAD	399	7	5	0.5	120	0.19	35	71	15	15	2
4691	BtG	median	6555	89	106	7.1	486	3.23	623	395	31	28	29
		MAD	233	7	4	0.8	41	0.33	40	65	8	5	1
4801	BtG	median	6560	83	115	9.2	517	0.17	93	481	71	38	27
		MAD	546	7	6	0.7	110	0.04	9	99	35	12	2
5471	BtG	median	5876	94	115	8.4	588	0.18	140	436	44	34	25
		MAD	547	6	6	0.9	43	0.06	16	109	19	15	1
4802	BtG	median	5527	129	129	22.4	937	0.21	99	356	134	40	29
		MAD	405	4	6	2.2	87	0.03	9	82	42	4	1
4692	BtG	median	5111	92	110	7.3	506	0.41	239	655	123	26	25
		MAD	521	6	8	0.8	56	0.05	31	85	35	6	2
4940	BtG	median	6265	51	84	5.5	402	1.37	232	530	78	20	17
		MAD	249	3	7	1.4	93	0.20	32	69	14	2	1
4941	BtG	median	4365	62	107	8.6	495	0.23	311	470	62	33	23
		MAD	606	11	13	1.4	152	0.13	68	126	21	13	2
4942	BtG	median	6823	76	114	8.5	381	0.30	477	581	47	33	22
		MAD	520	8	8	1.1	74	0.08	36	101	30	8	1
4693	BtG	median	6941	65	97	8.4	472	3.08	541	460	76	31	22
		MAD	289	6	7	1.4	69	0.25	22	89	16	5	2
5423	ZiGC	median	17,062	77	92	4.7	150	0.28	628	388	55	81	46
		MAD	989	8	14	1.2	91	0.13	419	118	26	27	6
5425	ZiGC	median	17,312	69	83	5.3	96	0.20	181	327	24	64	48
		MAD	2216	6	9	1.0	37	0.11	48	99	7	16	6
5427	GR	median	14,521	53	146	2.8	37	0.48	150	373	28	13	43
		MAD	1206	7	10	0.3	6	0.11	37	33	9	3	4
5428	GR	median	15,380	54	161	2.7	42	0.53	155	401	19	13	44
		MAD	790	7	25	0.7	10	0.11	32	42	9	3	4
5429	ZiGC	median	16,438	64	83	13.4	65	0.61	84	390	33	31	34
		MAD	336	3	6	1.2	12	0.07	12	26	7	4	2
5430	ZiGC	median	16,046	74	79	16.7	82	0.35	75	439	26	29	36
		MAD	1079	4	12	1.9	16	0.11	18	78	6	4	4
5438	GR	median	18,456	58	97	5.4	69	0.80	118	496	22	39	45
		MAD	906	5	8	0.7	14	0.10	30	29	13	5	3

(*continued on next page*)

Table 4 (*continued*)

Sample	Rock		Li	Sc	Ga	Ge	Nb	In	Sn	Cs	Ta	W	Tl
5434	ZiGC	median	16,620	74	77	4.7	66	0.24	44	366	31	28	34
		MAD	1408	9	12	0.7	20	0.06	16	101	12	8	7
5436	ZiGC	median	18,607	65	81	5.9	69	0.33	69	375	16	31	41
		MAD	988	14	8	0.9	32	0.14	25	96	7	12	5
4981	GR	median	16,024	61	160	5.6	45	5.79	176	477	17	20	40
		MAD	615	4	8	0.6	6	4.55	35	42	3	2	2
5412	QZV	median	18,688	46	105	4.3	37	0.90	121	382	10	29	39
		MAD	1185	3	6	0.3	3	0.10	24	35	2	5	2

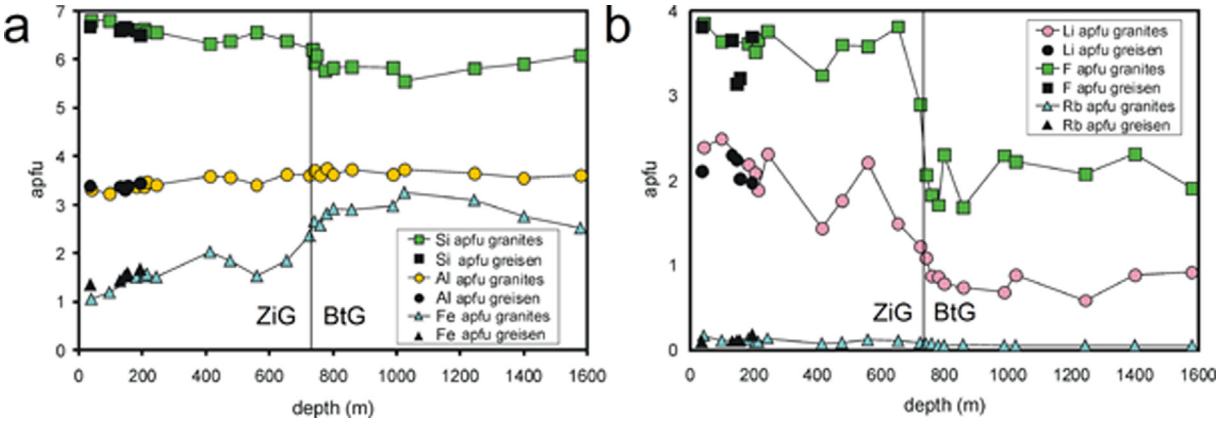

Fig. 7. Vertical zoning of mica composition in the borehole CS-1 (in apfu): a, Si, Al, Fe; b, Li, Rb, F.

granites and pegmatites cannot be analyzed using electron microprobe. To solve this problem, several methods of Li calculation from other elements, easily analyzed by the microprobe, have been suggested (Stone et al., 1988; Tindle and Webb, 1990; Tischendorf et al., 1997). In mineralogical practice, the Tischendorf's method [Li_2O (wt. %) = 0.298*SiO_2 (wt.%)–9.658] has been frequently applied (Li et al., 2015; Legros et al., 2018).

While Li enters the mica crystal lattice along several competing substitution schemes (annite–trilithionite, siderophyllite–polylithionite, muscovite–lepidolite), the Li content cannot be easily calculated based on formula stoichiometry; all suggested methods are based on statistical evaluation of large datasets of published chemical and microprobe analyses. This approach is useful for a first approximation but can result in significant errors in a particular case. Fig. 10a shows that, in the case of the studied Li-Fe micas from Cínovec, the values calculated according to Tischendorf are overestimated by 0.5–1 wt% in most samples. The real micas from Cínovec contain, at a given content of SiO_2, less Li than expected by ideal trioctahedral substitutions and also less Li than calculated using the Tischendorf's formula (Fig. 10b). This is caused by the higher-than-ideal content of Al in the trioctahedral layer: micas from Cínovec, and probably a large majority of Li-Fe micas worldwide, are not ideal trioctahedral micas containing some vacancies.

6.2. The share of mica in the bulk-rock budget of ore elements

Knowing the modal content of mica in the rock, the bulk-rock chemical composition, and the contents of particular elements in mica, we are able to compute the share of mica in the bulk-rock budget of these elements. This will be later used as a supporting argument for the discussion of processes forming the deposit.

Mica is the only host of Li in the Cínovec magmatic system, and an important host of F, Rb, Cs, Tl, Ga, Sn, W, Nb, Ta and Sc (Fig. 11). The actual F content in mica and the share of mica in F budget increase from the BtG to greisen (Fig. 11a): biotite accommodates 25–35% and zinnwaldite 25–100% of the present F, the rest being hosted especially by fluorite and topaz. While the contents of Ca available for fluorite crystallization decrease upwards, fluorine dominantly enters the crystal lattice of mica up to a 95% occupancy of the (F, OH)-site. A similar trend was also found in the case of Rb (Fig. 11b), Cs and Tl, all hosted also by K-feldspar. While the contents of Kfs decrease from BtG to ZiGC (Breiter et al., 2017a), all elements geochemically following potassium are dominantly accommodated in mica in ZiG and greisens. A different trend was found in the budget of Nb: the share of mica in Nb budget during the pluton evolution generally decreases from ca. 20–80% in the BtG to 2–10% in most samples of the ZiG and ZiGC. This means that in the less evolved BtG the major part of Nb was incorporated in mica and only a subordinate part into rutile. In the ZiG and ZiGC, the major part of Nb was hosted by accessory Nb-rich rutile and columbite, respectively (Breiter et al., 2017c), and the influence of later crystallizing mica on Nb distribution was minimized (Fig. 11c). The Nb share of zinnwaldite from greisen samples scattered: Nb-rich samples contain columbite and the share of mica in Nb budget is small. In unmineralized Nb-poor samples, however, it increases up to 50%. The shares of mica in the budget of Ta (Fig. 11d) and Sn (Fig. 11e) are similar to those in the budget of Nb. The share of mica in the budget of tungsten is only about 10% in the BtG and between 4 and 30% in the ZiG + ZiGC (Fig. 11f); a major part of W is probably hosted by an oxide mineral. The shares of mica in W budget in mineralized greisen samples containing wolframite and scheelite are always negligible.

6.3. Mica in the mineralizing process

Based on the vertical zoning of mica, its mineral assemblage, and the share of mica in the budget of F, Li and rare metals, we may try to interpret the role of mica in the origin of the deposit.

Zinnwaldite grains in greisen are homogeneous in BSE, which indicates their homogeneous chemical composition as regards the distribution of major elements. The contents of trace elements are scattered, but no regular zoning was identified. Consequently, remnants of primary magmatic zinnwaldite and later hydrothermal zinnwaldite grooving in the greisen stage cannot be distinguished. We conclude that all zinnwaldite in greisen was fully re-equilibrated in a reaction with

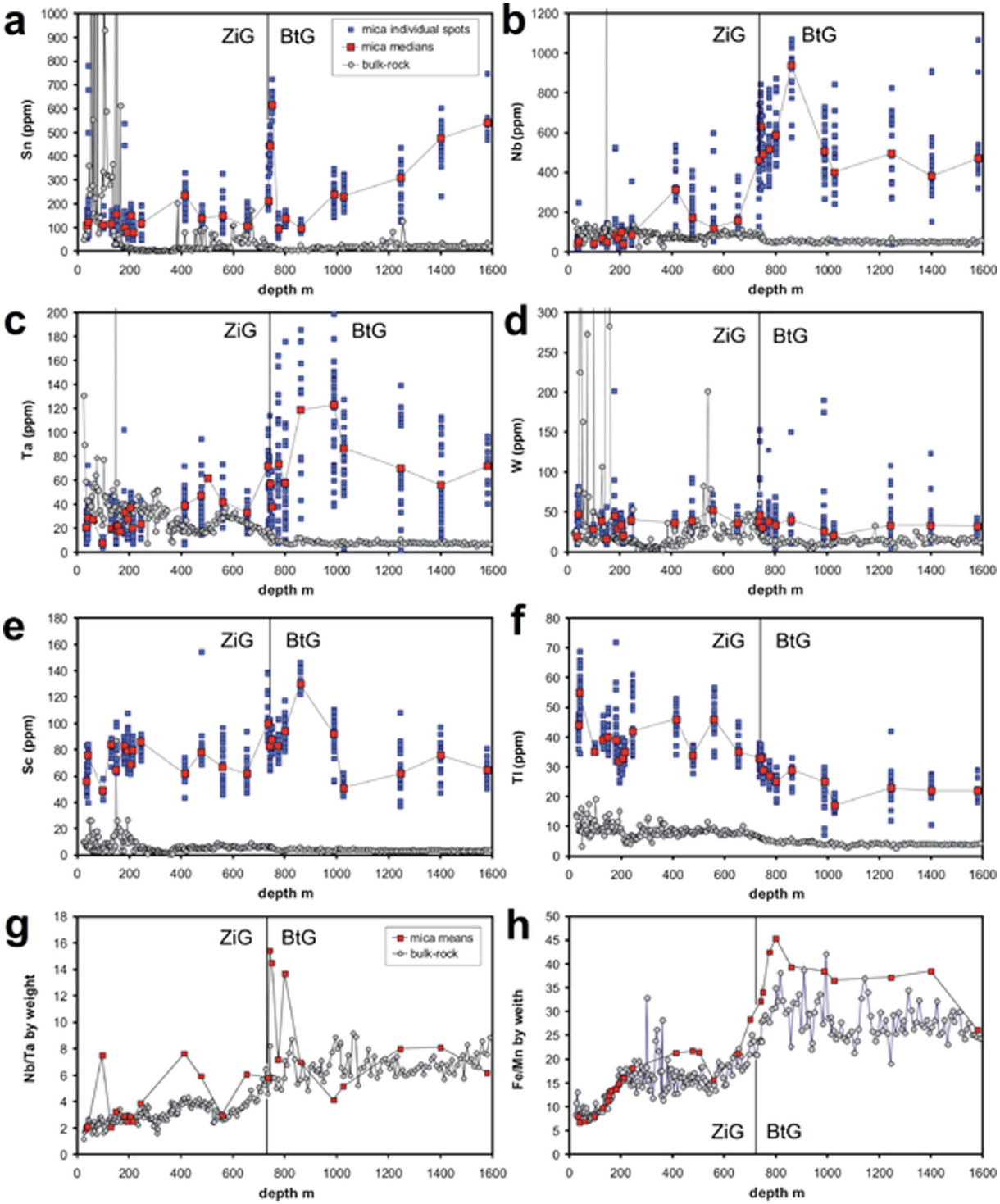

Fig. 8. Vertical zoning of mica composition in the borehole CS-1 (in ppm) compared with bulk-rock composition. All analyses (blue points) and medians (red points) are shown in diagrams a–f, while only medians are shown in diagrams g–h. Bulk-rock data are shown in gray: a, Sn; b, Nb; c, Ta; d, W; e, Sc; f, Tl;, g, Nb/Ta; h, Fe/Mn. (For interpretation of the references to colour in this figure legend, the reader is referred to the web version of this article.)

the greisenizing fluid. This is different from quartz, where magmatic cores and hydrothermal overgrowths can be easily distinguished using cathodoluminescence (Breiter et al., 2017d).

Comparing zinnwaldite from granite and these from greisen and veins, the latter is slightly poorer in FeO (means 11.5 *vs*. 12.8 wt%), Rb_2O (means 1.1 *vs*. 1.4 wt%) and F (means 7.2 *vs.* 7.8 wt%), and enriched in SiO_2 (means 46.8 *vs.* 45.8 wt%) and MnO (means 1.15 *vs.* 1.0 wt%). The contents of Li_2O are almost identical, about 3.6 wt%. The variability in trace element contents is higher: zinnwaldite from greisen and veins in borehole CS-1 is, compared to zinnwaldite from neighbouring granites, relatively depleted in Nb (54 *vs.* 63 ppm), W (26 *vs.* 41 ppm), Sn (86 *vs.* 115 ppm) and Cs (370 *vs.* 472 ppm), and enriched in Ga (94 *vs.* 72 ppm, in all cases means of all analyzed samples from the depth of 0–250 m). The contents of other measured trace elements differ insignificantly. In other words, mica crystallizing from fluid during greisenization was relatively enriched in Ga and, at the same time, impoverished in Rb, F, Sn and W in comparison with mica in granite.

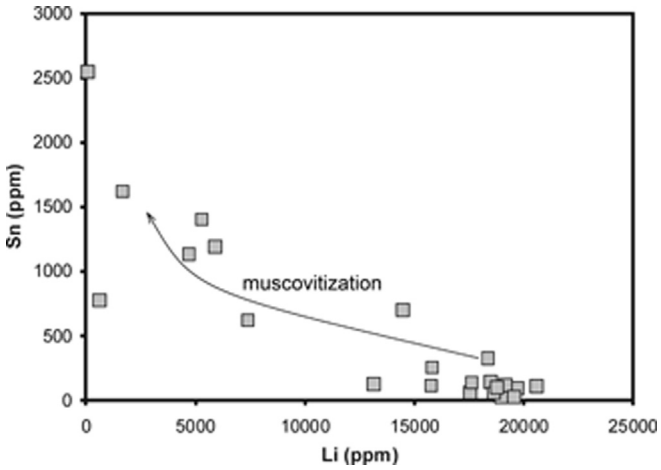

Fig. 9. Input of tin during muscovitization: contents of Li *vs.* Sn in muscovite.

Comparing zinnwaldite from greisen in the central part of the deposit (greisen selvages of quartz veins, altogether 165 analytical spots) with zinnwaldite from greisen in the southern part of the deposit (massive greisen bodies, 119 analytical spots), the former is slightly enriched in Li (17.350 *vs.* 16.640 ppm), Cs (437 *vs.* 390 ppm), Sn (197 *vs.* 130 ppm), W (46 *vs.* 29 ppm), Nb (133 *vs.* 107 ppm), Ta (31 *vs.* 24 ppm), and Sc (73 *vs.* 65 ppm). Zinnwaldite from the southern greisen is slightly enriched in Ga (112 *vs.* 81 ppm), while the contents of Ge and Tl are nearly the same (9 *vs.* 7 and 43 *vs.* 41 ppm, respectively, means of all available analyses in all cases). In relation with this difference, it is worth mentioning that the major greisen bodies in the south were described as geologically younger than greisen selvages along veins in the centre, having a different structural position in detail (Fengl et al., 1991; unpublished results of actual revision of the deposit by Geomet Co.). The systematic shift in the zinnwaldite composition from granites through greisen selvages to major greisen bodies corresponds to their relative age and thus to the expected decrease in their crystallization temperature.

Johan et al. (2012), studying micas from Cínovec, found that biotite is generally Sn-richer than zinnwaldite. This finding, although based on a very limited number of analyses, has led these authors to an opinion that Sn-rich biotite was the primary host of Sn; later, during the process of "lithionation", biotite in the whole upper rock packet (depth interval 0–735 m) was transformed to Sn-poor zinnwaldite + cassiterite. Our much larger dataset shows the following relation between the contents of Li *vs.* contents of rare metals and other trace elements (Fig. 12):

Among the analyzed elements, only Tl is well positively correlated with Li (Fig. 12a); this is consistent with the incompatible behaviour of these two elements in granitic melt (Shaw, 1957). In contrast, the contents of Nb, Ta and Sn (Fig. 12b, c, d) generally decrease with increasing Li, while no correlation was found between Li and Cs (Fig. 12e), W (Fig. 12f), Sc, Ga, and Ge. So, our data confirmed the negative correlation between Li and Sn mentioned by Johan et al. (2012), although we provide a different explanation for this fact.

In our opinion, Sn-rich biotite in biotite granites as well as Sn-poor zinnwaldite in zinnwaldite granites are primary magmatic minerals. The only documented hydrothermal alteration of zinnwaldite within the complex of zinnwaldite granites is muscovitization locally found in greisens (Fig. 6). This process, insignificant in its volume, led to the enrichment of mica in Sn and its depletion in Li (Fig. 9). This means that the process was the opposite to the Johan's et al. (2012) assumption.

The paradox that biotite from only slightly Sn-enriched biotite granites (usually 10–30 ppm Sn) shows higher Sn contents than zinnwaldite from strongly Sn-enriched zinnwaldite granites (usually 50–200 ppm Sn) can be explained by evaluating the whole mineral assemblages of both granite types and the order of crystallization of particular minerals. Biotite is, besides relatively scarce Ti-oxides, the major host of rare metals in biotite granites, while the generally low contents of Sn, Nb, and Ta in zinnwaldite from all facies of zinnwaldite granites should be explained by its relatively late crystallization when a substantial part of rare metals was already bound in disseminated magmatic cassiterite and columbite. During the greisen stage, rare metals preferably formed oxide minerals (Breiter et al., 2017c), and the associated zinnwaldite is Sn, Nb, Ta-poor.

The probable source of rare metals and Li and F necessary for the greisen formation was in the middle part of the complex of zinnwaldite granites, at depths of 260–369 m in borehole CS-1. Here, a body of quartz-feldspathitic rocks about 130 thick, extraordinarily poor in volatiles and metals ("mica-free granite"), is explained as alkali-rich remnant after fluid segregation from the residual melt. The released fluid rich in F and Li effectively sequestered Sn and W from the melt and transported those upwards forming zinnwaldite-rich greisen + oxide minerals (cassiterite, scheelite > wolframite, columbite, pyrochlore), while the residual silicate melt crystallized as volatile- and metal-poor mica-free granite (Breiter et al. 2017a,c).

Late muscovitization indicates the second, although spatially limited, episode of tin transfer to the upper part of the cupola. In Beauvoir, France, similar Sn-rich late muscovite in greisen is interpreted to

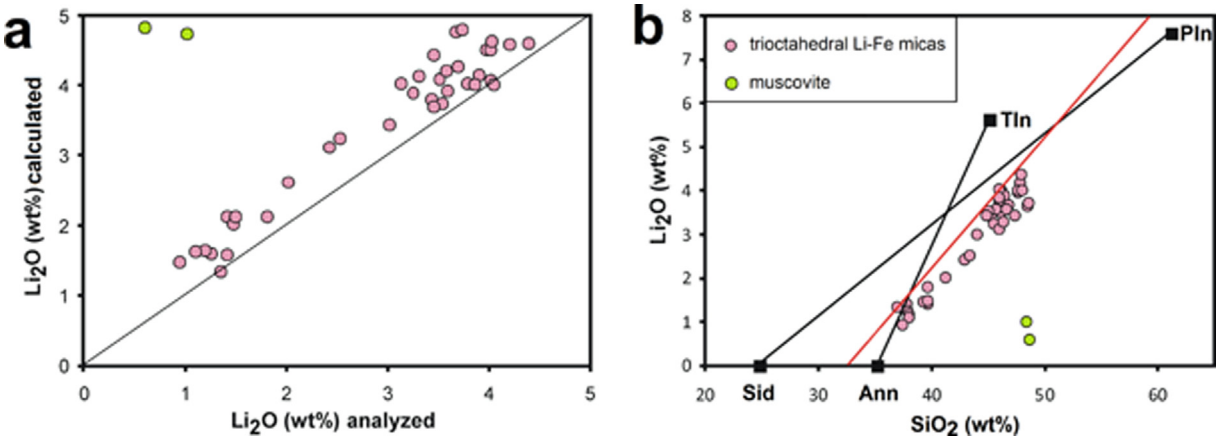

Fig. 10. Comparison of real Li contents in mica with those calculated according to Tischendorf et al. (1997): a, comparison of analyzed and calculated Li values of micas from Cínovec; b, A relation between the contents of SiO_2 and LiO_2 along ideal substitution series siderophyllite (Sid)–polylithionite (Pln) and annite (Ann)–trilithionite (Tln) is shown in black lines. Tischendorf's formula Li_2O (wt%) = 0.298*SiO_2 (wt%)–9.658 is shown in a red line. Note than nearly all calculated Li values are overestimated. (Keep on mind than the shown ideal substitution will be in reality slightly variable depending on F/OH- and Fe/Mn + Mg-values of the analyzed micas.)

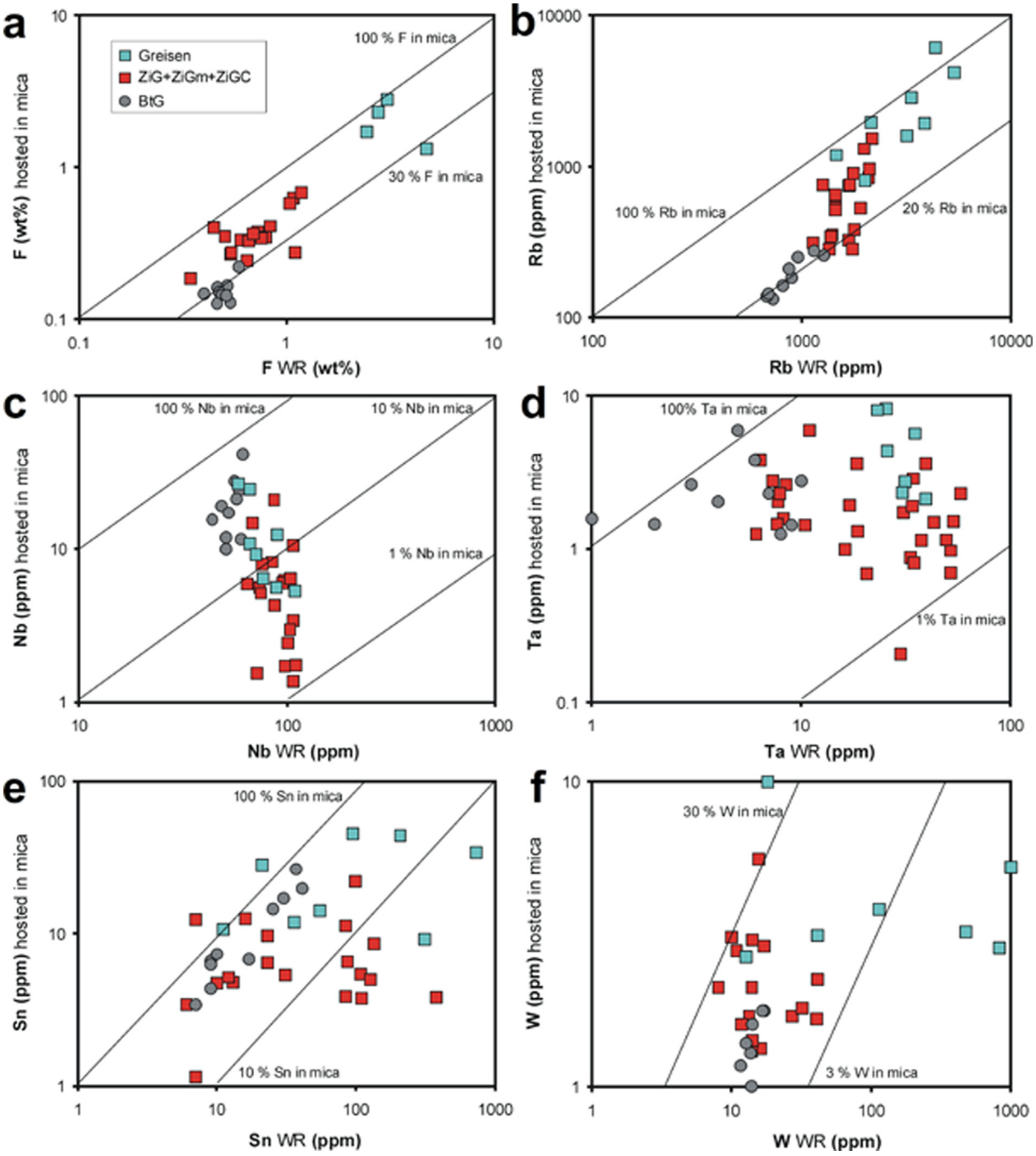

Fig. 11. The share of mica in the whole-rock (WR) budget of some elements: a, F; b, Rb; c, Nb; d, Ta; e, Sn; f, W.

incorporate tin from altered magmatic cassiterite (Monnier, 2018). At Cínovec, there is no evidence for cassiterite dilution in the cupola. The source of this fluid, poor in F and Li in this case, cannot be precisely localized; nevertheless, signs of muscovitization are limited to the uppermost part of the cupola above the zone of mica-free granites.

6.4. Comparison with Li-micas from other rare-metal granites

Despite of huge volumes of mica-related literature, papers with reliable datasets of major, Li, and trace element analyses of Li-rich micas from rare-metal granites or pegmatites are as yet scarce. Papers using modern spot analyses (EPMA + LA-ICP-MS) are effectively limited to Van Lichtervelde et al. (2008), Roda-Robles et al. (2012), Xie et al. (2015), Legros et al. (2016) and Breiter et al. (2017b). The contents of Li and trace elements in mica concentrates from pegmatites analyzed by a combination of chemical methods (XRF, AAS, ICP-OES) were published by Wise (1995). Identical methods were used by Monier et al. (1987) in Beauvoir, Stone et al. (1988) in Cornwall, du Bray (1994) in Saudi Arabia, Roda-Robles et al. (1995) and Vieira et al. (2011), both in Spain, and by Martins et al. (2012) in Portugal. All these data including author's unpublished LA-ICP-MS data from Beauvoir granite and western Erzgebirge are used for comparison with micas from Cínovec (Fig. 13). Among the compared granitic micas, all plutons except Beauvoir contain trioctahedral Li-Fe micas of the biotite–zinnwaldite series. In contrast, all referred LCT pegmatites contain dioctahedral micas of the muscovite–lepidolite series (Rieder et al., 1999). In the Beauvoir granite, trioctahedral Fe-poor micas of the zinnwaldite–trilithionite series prevail. These differences must be taken into account

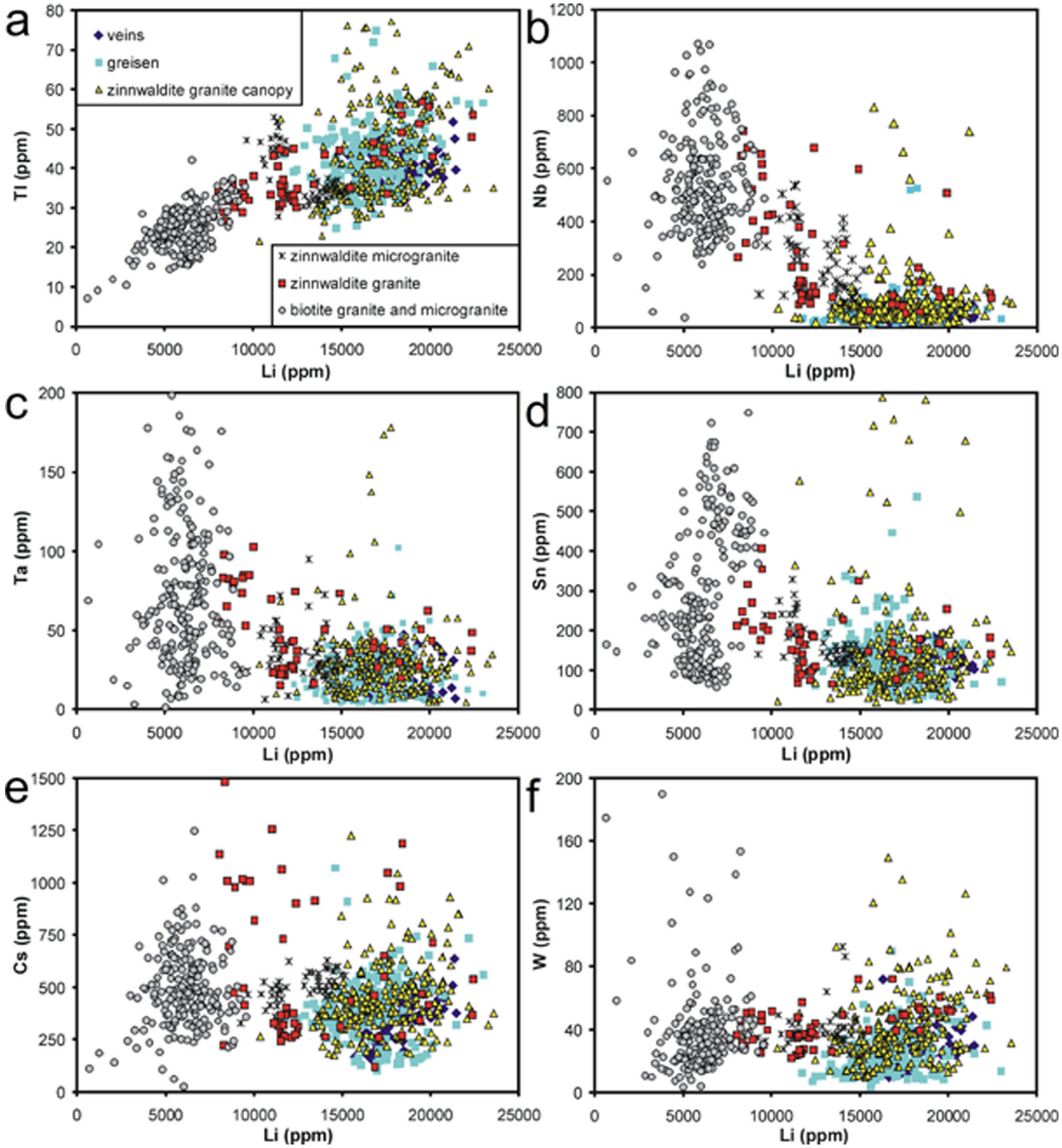

Fig. 12. A relation between the contents of Li and trace elements in trioctahedral micas: a, Li *vs.* Tl; b, Li *vs.* Nb; c, Li *vs.* Ta; d, Li *vs.* Sn; e, Li *vs.* Cs; f, Li *vs.* W.

discussing the contents of trace elements, as scarce studies comparing associated biotite and muscovite indicate higher potential of muscovite to accommodate Sn and probably also other HFSE (Koller and Breiter, 2003). In both, granite and pegmatite micas, Li closely positively correlates with fluorine: the equation F (wt%) ÷ 2*Li_2O (wt%) is valid up to ca. 4 wt% of Li_2O (nearly ideal zinnwaldite), where a nearly full F saturation is reached. With further increase in Li (zinnwaldite → lepidolite), F contents cannot increase any further (Fig. 13a). Several points located outside this trend (samples too poor in F) represent micas from amblygonite-spodumene pegmatites of the Fregeneda area in western Spain (Roda et al., 1995); these micas were analyzed as monomineral concentrates using AAS (Li) and XRF (F), which may indicate somewhat lower accuracy of data.

The contents of Nb in mica is relatively high and systematically decrease during the evolution of some granite plutons (Saudi Arabia, Cínovec) or are generally low in others (< 350 ppm: western Erzgebirge, Cornwall, China). Low Nb contents (mostly < 200 ppm) were found also in all referred pegmatitic muscovites (Fig. 13b). The behavior of W differs in individual plutons: W positively correlates with Li (from < 20 ppm in biotites to 150–300 ppm in zinnwaldite and lepidolite) in strongly peraluminous plutons like Beauvoir and western Erzgebirge and also in majority of referred pegmatites. In contrast, W contents remained comparatively low during the whole evolution of the Cínovec and Maoping plutons, and were highly variable in Yashan granites (Fig. 13c). The most complicated distribution was found for Sn (Fig. 13d). The only statement can be generally made for granites and pegmatites: Li-poor to moderately Li-enriched micas may be strongly enriched in Sn up to 1000 ppm, while Li-rich micas (> 3 wt% Li_2O) usually contain less than ca. 350 ppm Sn.

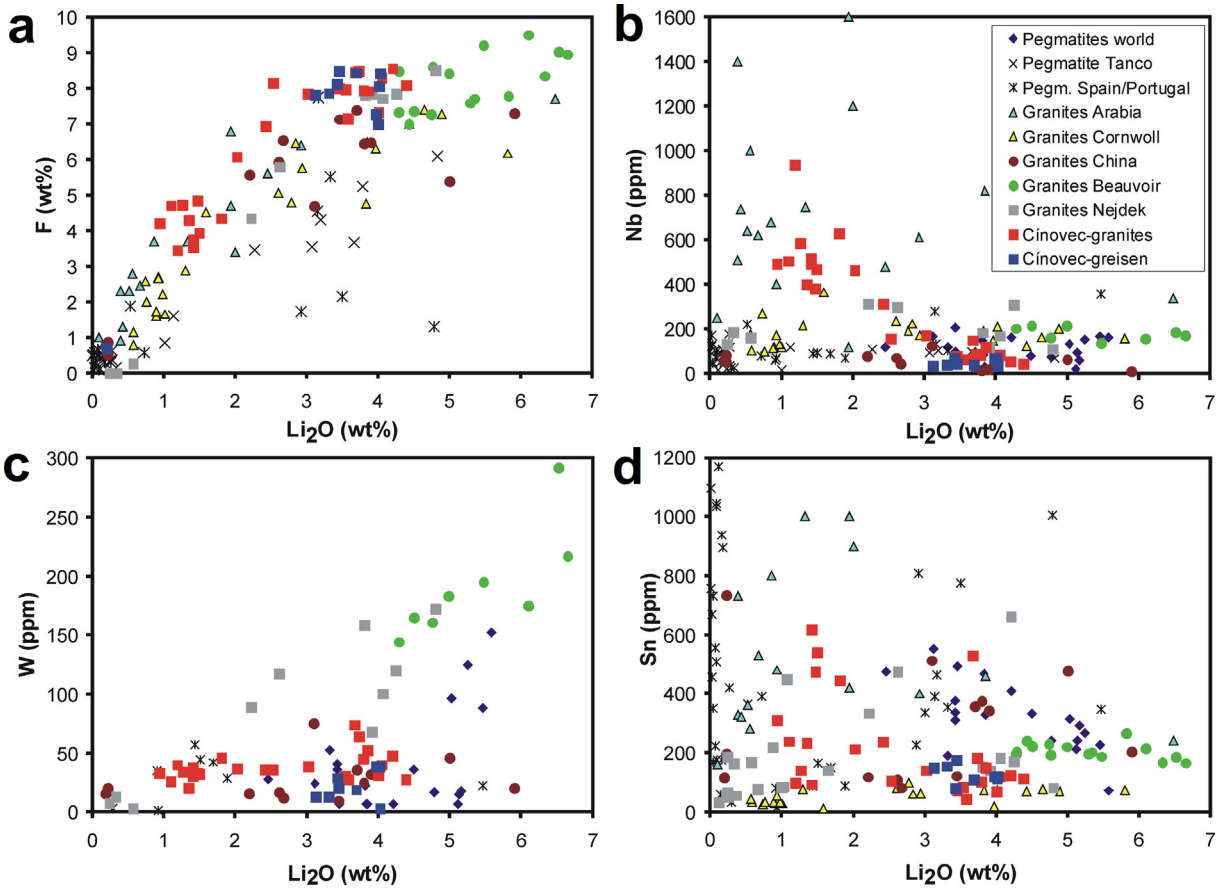

Fig. 13. Comparison of ore-element contents in micas from different granites and pegmatites: a, Li_2O *vs.* F; b, Li_2O *vs.* Nb; c, Li_2O *vs.* W; d, Li_2O *vs.* Sn. Source of data: Wise (1995) – Li-pegmatites worldwide; Van Lichtervelde et al. (2008) – Tanco pegmatite, Canada; Roda et al. (1995), Martins et al. (2012), Roda-Robles et al. (2012) and Vieira et al. (2011) – pegmatites from western Spain and eastern Portugal; du Bray (1994) – granites from Saudi Arabia; Monier et al. (1987) – Beauvoir granite, France; Stone et al. (1988) – granites from Cornwall; Xie et al. (2015) and Legros et al. (2016) – Yashan granites, China; author's data from the Nejdek pluton (western Erzgebirge) and Beauvoir, France.

7. Summary

Chemical composition of magmatic and hydrothermal micas along with whole-rock chemistry provide important information about the evolution of strongly fractionated rare-metal granite system necessary to formulate a reliable genetic scenario. In the case of the Cínovec deposit, the micas yielded following constraining information:

- all primary micas are trioctahedral micas of the annite–zinnwaldite–lepidolite series.
- vertical zoning (fractionation) of lithophile elements in mica including Li, Rb, and F well corroborate zoning of these elements in the bulk rock.
- the contents of HFSE in mica do not correspond to those in the bulk rock (melt). Generally, biotite associated only with Ti-oxides displays distinctly higher contents of Sn, Nb, Ta and W than zinnwaldite associated with cassiterite, columbite, and pyrochlore.
- the share of mica in the bulk-rock budget of Sn decreases from 40–70% in biotite granite to less than 5% in mineralized greisen; the shares of mica in budgets of Nb and Ta are lower but have identical trends. The entry of the HFSE to mica is mainly controlled by the order of crystallization of mica *vs.* accessory oxide minerals.
- during hydrothermal greisenization, primary magmatic zinnwaldite was fully re-equilibrated: slightly enriched in Si, Mn and Ga, and depleted in Fe, Rb, F, Cs and ore elements Sn, Nb, Ta and W.
- late local muscovitization in the upper part of the cupola was accompanied by an input of Sn. Late muscovite is Li, F-poor, and chemically strongly differs from remnants of greisen-stage zinnwaldite; no transitional composition between zinnwaldite and muscovite was found.
- we do not recommend to calculate Li contents in mica from microprobe data. Such calculation is subject to a large error.

Acknowledgements

This work was supported by the Czech Science Foundation, Czech Republic, project No. P210/14/13600S and conducted with institutional support RVO 67985831 of the Institute of Geology of the Czech Academy of Sciences. One anonymous reviewer is thanked for detail inspiring review.

References

Argollo, R.D., Schilling, J.G., 1978. Ge–Si and Ga–Al fractionation in Hawaian volcanic rocks. Geochim. Cosmochim. Acta 42, 623–630.
Bailey, S.W., (ed.), 1984. Micas. Reviews in Mineralogy 13, 584 pp.
Beskin, S.M., Grebennikov, A.M., Matias, V.V., 1994. The Khangilai granite pluton and related Orlovskoe tantalum deposit in Transbaikalia. Petrology 2, 68–87.
du Bray, E.A., 1994. Compositions of micas in peraluminous granitoids of the eastern Arabian Shield. Contrib. Mineral. Petrol. 116, 381–397.
Brigatti, M.F., Lugli, C., Poppi, L., Ford, E.E., Kile, D.E., 2000. Crystal chemical variations in Li- and Fe-rich micas from Pikes Peak batholith (central Colorado). Am. Mineral. 85, 1275–1286.
Breiter, K., 1997. Teplice rhyolite (Krušné hory Mts., Czech Republic) chemical evidence of a multiply exhausted stratified magma chamber. Bull. Czech Geol. Surv. 72, 205–213.
Breiter, K., Gardenová, N., Kanický, V., Vaculovič, T., 2013. Gallium and germanium geochemistry during magmatic fractionation and post-magmatic alteration in

different types of granitoids: a case study from the Bohemian Massif, Czech Republic. Geol. Carpathica 64, 171–180.
Breiter, K., Ďurišová, J., Hrstka, T., Korbelová, Z., Hložková, Vaňková M., Vašinová, Galiová M., Kanický, V., Rambousek, P., Knésl, I., Dobeš, P., Dosbaba, M., 2017a. Assessment of magmatic *vs.* metasomatic processes in rare-metal granites: a case study of the Cínovec/Zinnwald Sn-W-Li deposit, Central Europe. Lithos 292–293, 198–217.
Breiter, K., Vaňková, M., Vašinová Galiová, M., Korbelová, Z., Kanický, V., 2017b. Lithium and trace element concentrations in trioctahedral micas from granites of different geochemical types measured via laser ablation ICP-MS. Mineral. Mag. 81, 15–33.
Breiter, K., Korbelová, Z., Chládek, Š., Uher, P., Knesl, I., Rambousek, P., Honig, S., Šešulka, V., 2017c. Diversity of Ti–Sn–W–Nb–Ta oxide minerals in the classic granite-related magmatic–hydrothermal Cínovec/Zinnwald Sn–W–Li deposit (Czech Republic). Eur. J. Mineral. 29, 727–738.
Breiter, K., Ďurišová, J., Dosbaba, M., 2017d. Quartz chemistry – a step to understanding magmatic-hydrothermal processes in ore-bearing granites: Cínovec/Zinnwald Sn-W-Li deposit, Central Europe. Ore Geol. Rev. 90, 25–35.
Černý, P., Meintzer, R.E., Anderson, A.J., 1985. Extreme fractionation in rare-element granitic pegmatites: selected examples of data and mechanisms. Can. Mineral. 23, 381–421.
Fengl, M. et al., 1991. Final shut down report of Cínovec mining. Manuscript, Archive of the Czech Geological Survey- Geofond. (in Czech).
Foster, M.D., 1960. Interpretation of the composition of Li-micas. U.S. Geol. Surv. Prof. Pap. 354E, 113–147.
Haidinger, W., 1845. Handbuch der bestimmenden Mineralogie. Braumüller & Seidel, Wien, pp. 625.
Hoth, K., Wasternack, J., Berger, H.-J., Breiter, K., Mlčoch, B., Schovánek, P., 1995. Geologische Karte Erzgebirge/Vogtland 1:100 000. Sachsisches Landesamt für Umvelt und Geologie Freiberg.
Johan, Z., Strnad, L., Johan, V., 2012. Evolution of the Cínovec (Zinnwald) granite cupola, Czech Republic: composition of feldspars and micas, a clue to origin of W, Sn mineralization. Can. Mineral. 50, 1131–1148.
Kempe, U., Wolf, D., 2006. Anomalously high Sc contents in ore minerals from Sn-W deposits: possible economic significance and genetic implications. Ore Geol. Rev. 28, 103–122.
Koller, F., Breiter, K., 2003. Variation of Li-, Be-, Rb-, and Sn-contents in micas from Variscan granites of the South Bohemian Pluton. In: International Symposium on Light Elements in Rock-forming Minerals. Nové Město na Moravě, Czech Republic, June 20–25. pp. 40–41.
Legros, H., Marignac, Ch., Mercadier, J., Cuney, M., Richard, A., Wang, R.-Ch., Charles, N., Lespinasse, M.-Y., 2016. Detailed paragenesis and Li-mica compositions as recorders of the magmatic-hydrothermal evolution of the Maoping W-Sn deposit (Jiangxi, China). Lithos 264, 108–124.
Legros, H., Marignac, C., Tabary, T., Mercadier, J., Richard, A., Cuney, M., Wang, R., Charles, N., Lespinasse, M., 2018. The ore-forming magmatic-hydrothermal system of the Piaotang W-Sn deposit (Jiangxi, China) as seen from Li-mica geochemistry. Am. Mineral. 103, 39–54.
Li, J., Huang, X.-L., He, P.-L., Li, W.-X., Yu, Y., Chen, L., 2015. In situ analyses of micas in the Yashan granite, South China: constraints on magmatic and hydrothermal evolutions of W and Ta-Nb bearing granites. Ore Geol. Rev. 65, 793–810.
Martins, T., Roda-Robles, E., Lima, A., Parseval, P., 2012. Geochemistry and evolution of micas in the Barroso-Alvao pegmatite field, Northern Portugal. Can. Mineral. 50, 1117–1129.
Merlet, C., 1994. An accurate computer correction program for quantitative electron probe microanalysis. Microchim. Acta 114 (115), 363–376.
Mlčoch, B., Skácelová, Z., 2010. Geometry of the Altenberg-Teplice caldera revealed by the borehole and seismic data in its Czech part. J. Geosci. 55, 217–229.
Monier, G., Charoy, B., Cuney, M., Ohnenstetter, D., Robert, J.L., 1987. Évolution spatiale et temporelle de la composition des micas du granite albitique a topaze-lepidolite de Beauvoir. Geol. France 1987, 179–188.
Monnier, L., 2018. Utilisation de la signature LA-ICPMS des quartz et des micas pour la reconstitution du fonctionnement d́un systeme magmatique et hydrothermal polyphasé. Application au complexe Sn-1 d́Echassieres (Massif Central, France). Doctoral thesis. University Paul Sabatier, Toulouse.
Petrík, I., Čík, Š., Miglierini, M., Vaculovič, T., Dianiška, I., Ozdín, D., 2014. Alpine oxidation of lithium micas in Permian S-type granites (Gemeric unit, Western Carpathians, Slovakia). Mineral. Mag. 78, 507–533.
Raimbault, L., Cuney, M., Azencott, C., Duthou, J.L., Joron, J.L., 1995. Geochemical evidence for a multistage magmatic genesis of Ta-Sn-Li mineralization in the granite at Beauvoir, French Massif Central. Econ. Geol. 90, 548–596.
Rieder, M., Hybler, J., Smrčok, L., Weiss, Z., 1996. Refinement of the crystal structure of zinnwaldite $2M_1$. Eur. J. Mineral. 8, 1241–1248.
Rieder, M., Cavazzini, G., Dyakonov, Y.S., Frank-Kamenetskii, V.A., Gottardi, G., Guggenheim, S., Koval, P.V., Muller, G., Neiva, A.M.R., Radoslovich, E.W., Robert, J.L., Sassi, P.F., Takeda, H., Weiss, Z., Wones, D.R., 1999. Nomenclature of micas. Mineral. Mag. 73, 267–279.
Roda, E., Pesquera, A., Velasco, F., 1995. Micas of the muscovite-lepidolite series from the Fregenada pegmatites (Salamanca, Spain). Mineral. Petrol. 55, 145–157.
Roda-Robles, E., Pesquera, A., Gil-Grespo, P., Torres-Ruiz, J., 2012. From granite to highly evolved pegmatite: a case study of the Pinilla de Fermoselle granite-pegmatite system (Zamora, Spain). Lithos 153, 192–207.
Seifert, T., Sandmann, D., 2006. Mineralogy and geochemistry of indium-bearing polymetallic vein-type deposits: Implications for host minerals from the Freiberg district Eastern Erzgebirge, Germany. Ore Geol. Rev. 28, 1–31.
Seltmann, R., Wetzel, H.-U., Felix, M., Schilka, W., 1987. Brekzien der Altenberger Scholle. Exkursion Führer 34. Jahrestagung der Gessellschaft für geologische Wissenschaften DDR, Berlin.
Shaw, D.M., 1957. The geochemistry of gallium, indium, thallium – a review. Phys. Chem. Earth 2, 548–596.
Stone, M., Exley, C.S., George, M.C., 1988. Composition of trioctahedral micas in the Cornubian batholith. Mineral. Mag. 52, 175–192.
Syritso, L.F., Tabuns, E.V., Volkova, E.V., Badanina, E.V., Vysotskii, Yu.A., 2001. Model for the genesis of Li-F granites in the Orlovka Massif, Eastern Transbaikalia. Petrology 9, 313–336.
Štemprok, M., Šulcek, Z., 1969. Geochemical profile through an ore-bearing lithium granite. Econ. Geol. 64, 392–404.
Tindle, A.G., Webb, P.C., 1990. Estimation of lithium contents in trioctahedral micas using microprobe data: application to micas from granitic rocks. Eur. J. Mineral. 2, 595–610.
Tischendorf, G., Gottesmann, B., Förster, H.J., Trumbull, R.B., 1997. On Li-bearing micas: estimating Li from electron microprobe analyses and an improved diagram for graphical representation. Mineral. Mag. 61, 809–834.
Van Lichtervelde, M., Grégoire, M., Linnen, R.L., Béziat, D., Salvi, S., 2008. Trace element geochemistry by laser ablation ICP-MS of micas associated with Ta mineralization in the Tanco pegmatite, Manitoba, Canada. Contrib. Mineral. Petrol. 155, 791–806.
Vieira, R., Roda-Robles, E., Pesquera, A., Lima, A., 2011. Chemical variation and significance of micas from the Fregeneda-Almendra pegmatitic field (Central-Iberian Zone, Spain and Portugal. Am. Mineral. 96, 637–645.
Walther, D., Breitkreuz, C., Rapprich, V., Kochergina, Y.V., Chlupáčová, M., Lapp, M., Stanek, K., Magna, T., 2016. The Late Carboniferous Schönfeld-Altenberg Depression on the NW margin of the Bohemian Massif (Germany/Czech Republic): volcanosedimentary and magmatic evolution. J. Geosci. 61, 371–393.
Weiss, Z., Rieder, M., Smrčok, L., Petříček, V., Bailey, S.W., 1993. Refinement of the crystal structures of two “protolithionites”. Eur. J. Mineral. 5, 493–502.
Wise, M.A., 1995. Trace element chemistry of lithium-rich micas from rare-element granitic pegmatites. Mineral. Petrol. 55, 203–215.
Xie, L., Wang, R.C., Groat, L.A., Zhu, J.C., Huang, F.F., Cempírek, J., 2015. A combined EMPA and LA-ICP-MS study of Li-bearing mica and Sn-Ti oxide minerals from the Qiguling topaz rhyolite (Qitianling District, China): the role of fluorine in origin of tin mineralization. Ore Geol. Rev. 65, 779–792.
Yin, L., Pollard, P.J., Shouxi, H., Taylor, R.G., 1995. Geologic and geochemical characteristics of the Yichun Ta-Nb-Li deposit, Jiangxi province, South China. Econ. Geol. 90, 577–585.